

The metabolite α -ketoglutarate extends lifespan by inhibiting ATP synthase and TOR

Randall M. Chin¹, Xudong Fu², Melody Y. Pai^{1*}, Laurent Vergnes^{3*}, Heejun Hwang^{2*}, Gang Deng⁴, Simon Diep², Brett Lomenick², Vijaykumar S. Meli⁵, Gabriela C. Monsalve⁵, Eileen Hu², Stephen A. Whelan⁶, Jennifer X. Wang⁷, Gwanghyun Jung², Gregory M. Solis⁸, Farbod Fazlollahi⁹, Chitrada Kaweeteerawat¹⁰, Austin Quach², Mahta Nili¹¹, Abby S. Krall², Hilary A. Godwin¹⁰, Helena R. Chang⁶, Kym F. Faull⁹, Feng Guo⁵, Meisheng Jiang², Sunia A. Trauger⁷, Alan Saghatelian¹², Daniel Braas^{2,13}, Heather R. Christofk^{2,13}, Catherine F. Clarke^{1,4}, Michael A. Teitel^{1,11}, Michael Petrascheck⁸, Karen Reue^{1,3}, Michael E. Jung^{1,4}, Alison R. Frand⁵ & Jing Huang^{1,2}

Metabolism and ageing are intimately linked. Compared with *ad libitum* feeding, dietary restriction consistently extends lifespan and delays age-related diseases in evolutionarily diverse organisms^{1,2}. Similar conditions of nutrient limitation and genetic or pharmacological perturbations of nutrient or energy metabolism also have longevity benefits^{3,4}. Recently, several metabolites have been identified that modulate ageing^{5,6}; however, the molecular mechanisms underlying this are largely undefined. Here we show that α -ketoglutarate (α -KG), a tricarboxylic acid cycle intermediate, extends the lifespan of adult *Caenorhabditis elegans*. ATP synthase subunit β is identified as a novel binding protein of α -KG using a small-molecule target identification strategy termed drug affinity responsive target stability (DARTS)⁷. The ATP synthase, also known as complex V of the mitochondrial electron transport chain, is the main cellular energy-generating machinery and is highly conserved throughout evolution^{8,9}. Although complete loss of mitochondrial function is detrimental, partial suppression of the electron transport chain has been shown to extend *C. elegans* lifespan^{10–13}. We show that α -KG inhibits ATP synthase and, similar to ATP synthase knockdown, inhibition by α -KG leads to reduced ATP content, decreased oxygen consumption, and increased autophagy in both *C. elegans* and mammalian cells. We provide evidence that the lifespan increase by α -KG requires ATP synthase subunit β and is dependent on target of rapamycin (TOR) downstream. Endogenous α -KG levels are increased on starvation and α -KG does not extend the lifespan of dietary-restricted animals, indicating that α -KG is a key metabolite that mediates longevity by dietary restriction. Our analyses uncover new molecular links between a common metabolite, a universal cellular energy generator and dietary restriction in the regulation of organismal lifespan, thus suggesting new strategies for the prevention and treatment of ageing and age-related diseases.

To gain insight into the regulation of ageing by endogenous small molecules, we screened normal metabolites and aberrant disease-associated metabolites for their effects on adult lifespan using the *C. elegans* model. We discovered that the tricarboxylic acid (TCA) cycle intermediate α -KG (but not isocitrate or citrate) delays ageing and extends the lifespan of *C. elegans* by ~50% (Fig. 1a and Extended Data Fig. 1a). In the cell, α -KG (or 2-oxoglutarate; Fig. 1b) is produced from isocitrate by oxidative decarboxylation catalysed by isocitrate dehydrogenase (IDH). α -KG can also be produced anaplerotically from glutamate by oxidative

deamination using glutamate dehydrogenase, and as a product of pyridoxal phosphate-dependent transamination reactions in which glutamate is a common amino donor. α -KG extended the lifespan of wild-type N2 worms in a concentration-dependent manner, with 8 mM α -KG producing the maximal lifespan extension (Fig. 1c); 8 mM was the concentration used in all subsequent *C. elegans* experiments. There is a ~50% increase in α -KG concentration in worms on 8 mM α -KG plates compared with those on vehicle plates (Extended Data Fig. 1b), or ~160 μ M versus ~110 μ M assuming homogenous distribution (Methods). α -KG not only extends lifespan, but also delays age-related phenotypes, such as the decline in rapid, coordinated body movement (Supplementary Videos 1 and 2). α -KG supplementation in the adult stage is sufficient for longevity (Extended Data Fig. 1c).

The dilution or killing of the *C. elegans* bacterial food source has been shown to extend worm lifespan¹⁴, but the lifespan increase by α -KG is not due to altered bacterial proliferation or metabolism (Fig. 1d, e and Extended Data Fig. 1d). Animals also did not view α -KG-treated food as less favourable (Extended Data Fig. 1e, f), and there was no significant change in food intake, pharyngeal pumping, foraging behaviour, body size or brood size in the presence of α -KG (Extended Data Fig. 1e–h; data not shown).

In the cell, α -KG is decarboxylated to succinyl-CoA and CO₂ by α -KG dehydrogenase (encoded by *ogdh-1*), a key control point in the TCA cycle. Increasing α -KG levels by *ogdh-1* RNA interference (RNAi) (Extended Data Fig. 1b) also extends worm lifespan (Fig. 1f and Supplementary Notes), consistent with a direct effect of α -KG on longevity independent of bacterial food.

To investigate the molecular mechanism(s) of longevity by α -KG, we took advantage of an unbiased biochemical approach, DARTS⁷. As we proposed that key target(s) of α -KG are likely to be conserved and ubiquitously expressed, we used a human cell line (Jurkat) that is easy to culture as the protein source for DARTS (Fig. 2a). Mass spectrometry identified ATP5B, the β subunit of the catalytic core of the ATP synthase, among the most abundant and enriched proteins present in the α -KG-treated sample (Extended Data Table 1); the homologous α subunit ATP5A was also enriched but to a lesser extent. The interaction between α -KG and ATP5B was verified using additional cell lines (Fig. 2b; data not shown), and corroborated for the *C. elegans* orthologue ATP-2 (Extended Data Fig. 2a).

α -KG inhibits the activity of complex V, but not complex IV, from bovine heart mitochondria (Fig. 2c and Extended Data Fig. 2b; data not

¹Molecular Biology Institute, University of California Los Angeles, Los Angeles, California 90095, USA. ²Department of Molecular and Medical Pharmacology, University of California Los Angeles, Los Angeles, California 90095, USA. ³Department of Human Genetics, University of California Los Angeles, Los Angeles, California 90095, USA. ⁴Department of Chemistry and Biochemistry, University of California Los Angeles, Los Angeles, California 90095, USA. ⁵Department of Biological Chemistry, University of California Los Angeles, Los Angeles, California 90095, USA. ⁶Small Molecule Mass Spectrometry Facility, FAS Division of Science, Harvard University, Cambridge, Massachusetts 02138, USA. ⁷Department of Chemical Physiology, The Scripps Research Institute, La Jolla, California 92037, USA. ⁸Pasarow Mass Spectrometry Laboratory, Department of Psychiatry and Biobehavioral Sciences and Semel Institute for Neuroscience and Human Behavior, University of California Los Angeles, Los Angeles, California 90095, USA. ¹⁰Department of Environmental Health Sciences, University of California Los Angeles, Los Angeles, California 90095, USA. ¹¹Department of Pathology and Laboratory Medicine, University of California Los Angeles, Los Angeles, California 90095, USA. ¹²Department of Chemistry and Chemical Biology, Harvard University, Cambridge, Massachusetts 02138, USA. ¹³UCLA Metabolomics Center, University of California Los Angeles, Los Angeles, California 90095, USA.

*These authors contributed equally to this work.

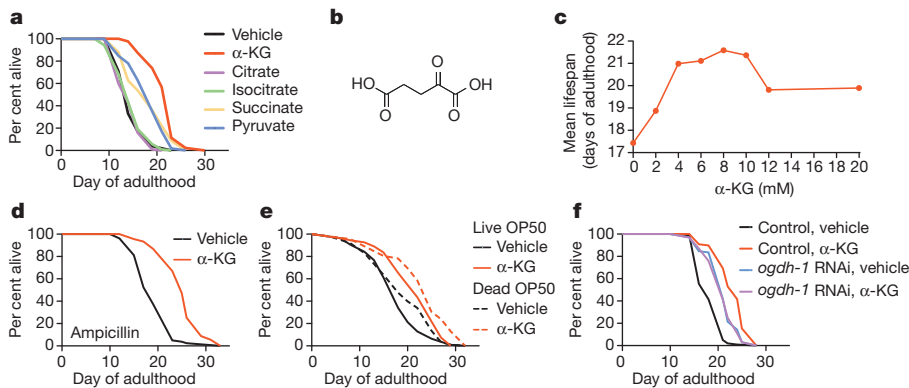


Figure 1 | α -KG extends the adult lifespan of *C. elegans*. **a**, α -KG extends the lifespan of adult worms in the metabolite longevity screen. All metabolites were given at a concentration of 8 mM. **b**, Structure of α -KG. **c**, Dose-response curve of the α -KG effect on longevity. **d**, **e**, α -KG extends the lifespan of worms fed bacteria that have been ampicillin arrested, mean lifespan (days of adulthood) with vehicle treatment (m_{veh}) = 19.4 ($n = 80$ animals tested),

shown). This inhibition is also readily detected in live mammalian cells (Fig. 2d; data not shown) and in live nematodes (Fig. 2e), as evidenced by reduced ATP levels. Concomitantly, oxygen consumption rates are lowered (Fig. 2f, g), similar to with *atp-2* knockdown (Extended Data Fig. 2c). Specific inhibition of complex V—but not the other electron transport chain (ETC) complexes—by α -KG is further confirmed by respiratory control analysis¹⁵ (Fig. 2h and Extended Data Fig. 2d–h). To understand the mechanism of inhibition by α -KG, we studied the enzyme inhibition kinetics of ATP synthase. α -KG (released from octyl

$m_{\text{KG}} = 25.1$ ($n = 91$), $P < 0.0001$ (log-rank test) (**d**); or γ -irradiation-killed, $m_{\text{veh}} = 19.0$ ($n = 88$), $m_{\text{KG}} = 23.0$ ($n = 46$), $P < 0.0001$ (log-rank test) (**e**). *OP50*, *E. coli* OP50 strain. **f**, α -KG does not further extend the lifespan of *ogdh-1* RNAi worms, $m_{\text{veh}} = 21.2$ ($n = 98$), $m_{\text{KG}} = 21.1$ ($n = 100$), $P = 0.65$ (log-rank test).

α -KG) decreases both the effective velocity of the enzyme-catalysed reaction at an infinite concentration of the substrate (V_{\max}) and the Michaelis constant (K_m) of ATP synthase, indicative of uncompetitive inhibition (Fig. 2i and Supplementary Notes).

To determine the significance of ATP-2 to the longevity by α -KG, we measured the lifespan of *atp-2* RNAi adults given α -KG. As reported previously¹³, *atp-2* RNAi animals live longer than control RNAi animals (Fig. 3a). However, their lifespan is not further extended by α -KG (Fig. 3a), indicating that ATP-2 is required for the longevity benefit of

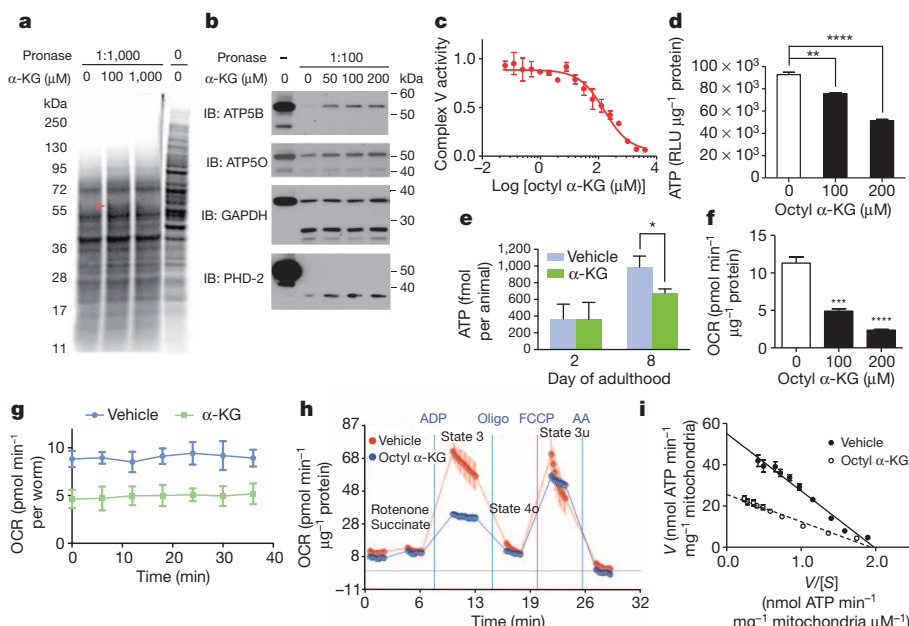


Figure 2 | α -KG binds and inhibits ATP synthase. **a**, DARTS identifies ATP5B as an α -KG-binding protein. Red arrowhead, protected band. **b**, DARTS confirms α -KG binding specifically to ATP5B. IB, immunoblot. **c**, Inhibition of ATP synthase by α -KG (released from octyl α -KG; Supplementary Notes). This inhibition was reversible (data not shown). **d**, **e**, Reduced ATP levels in octyl α -KG-treated normal human fibroblasts ($**P = 0.0016$, $****P < 0.0001$; by *t*-test, two-tailed, two-sample unequal variance) (**d**) and α -KG-treated worms (day 2, $P = 0.969$; day 8, $*P = 0.012$; by *t*-test, two-tailed, two-sample unequal variance) (**e**). RLU, relative luminescence units. **f**, **g**, Decreased oxygen consumption rate (OCR) in octyl α -KG-treated cells ($***P = 0.0004$, $****P < 0.0001$; by *t*-test, two-tailed, two-sample unequal variance) (**f**) and α -KG-treated worms ($P < 0.0001$; by *t*-test, two-tailed, two-sample unequal variance) (**g**). **h**, α -KG, released from

octyl α -KG (800 μ M), decreases state 3, but not state 4 or 3u ($P = 0.997$), respiration in mitochondria isolated from mouse liver. The respiratory control ratio is decreased in the octyl α -KG- (3.1 \pm 0.6) versus vehicle-treated mitochondria (5.2 \pm 1.0) ($*P = 0.015$; by *t*-test, two-tailed, two-sample unequal variance). Oligo, oligomycin; FCCP, carbonyl cyanide-4-(trifluoromethoxy)phenylhydrazone; AA, antimycin A. **i**, Eadie–Hofstee plot of steady-state inhibition kinetics of ATP synthase by α -KG (produced by *in situ* hydrolysis of octyl α -KG). [S] is the substrate (ADP) concentration, and V is the initial velocity of ATP synthesis in the presence of 200 μ M octanol (vehicle control) or octyl α -KG. α -KG (produced from octyl α -KG) decreases the apparent V_{\max} (53.9 to 26.7) and K_m (25.9 to 15.4), by nonlinear regression least-squares fit. **c–i**, Results were replicated in two independent experiments. Mean \pm standard deviation (s.d.) is plotted in all cases.

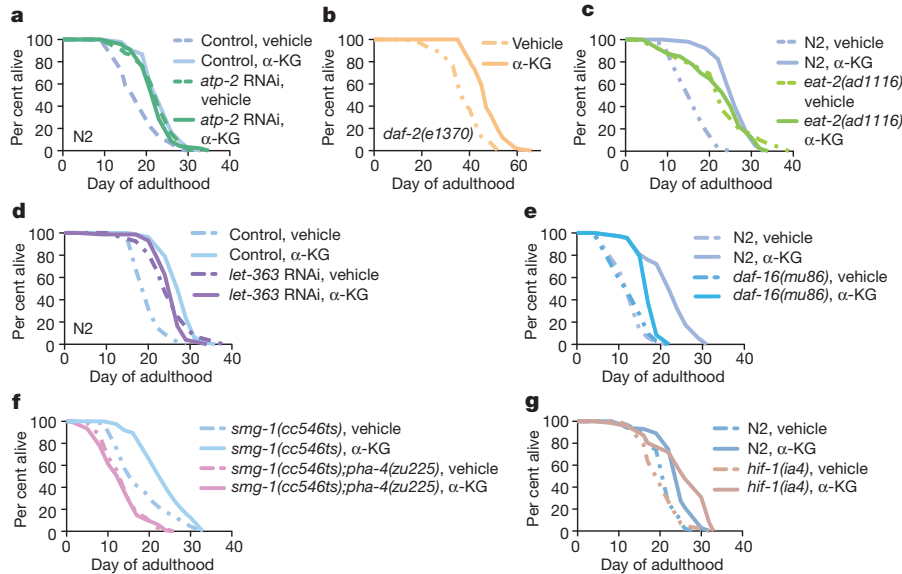


Figure 3 | α -KG longevity is mediated through ATP synthase and the dietary restriction/TOR axis. **a–g**, Effect of α -KG on the lifespan of mutant or RNAi worms. **a**, *atp-2* RNAi, $m_{\text{veh}} = 22.8$ ($n = 97$), $m_{\alpha\text{-KG}} = 22.5$ ($n = 94$), $P = 0.35$; or RNAi control, $m_{\text{veh}} = 18.6$ ($n = 94$), $m_{\alpha\text{-KG}} = 23.4$ ($n = 91$), $P < 0.0001$. **b**, *daf-2(e1370)*, $m_{\text{veh}} = 38.0$ ($n = 72$), $m_{\alpha\text{-KG}} = 47.6$ ($n = 69$), $P < 0.0001$. **c**, *eat-2(ad1116)*, $m_{\text{veh}} = 22.8$ ($n = 59$), $m_{\alpha\text{-KG}} = 22.9$ ($n = 40$), $P = 0.79$. **d**, *let-363* RNAi, $m_{\text{veh}} = 25.1$ ($n = 96$), $m_{\alpha\text{-KG}} = 25.7$ ($n = 74$), $P = 0.95$; or *gfp* RNAi control, $m_{\text{veh}} = 20.2$ ($n = 99$), $m_{\alpha\text{-KG}} = 27.7$ ($n = 81$),

$P < 0.0001$. **e**, *daf-16(mu86)*, $m_{\text{veh}} = 13.4$ ($n = 71$), $m_{\alpha\text{-KG}} = 17.4$ ($n = 72$), $P < 0.0001$; or N2, $m_{\text{veh}} = 13.2$ ($n = 100$), $m_{\alpha\text{-KG}} = 22.3$ ($n = 104$), $P < 0.0001$. **f**, *pha-4(zu225)*, $m_{\text{veh}} = 14.2$ ($n = 94$), $m_{\alpha\text{-KG}} = 13.5$ ($n = 109$), $P = 0.55$. **g**, *hif-1(i4)*, $m_{\text{veh}} = 20.5$ ($n = 85$), $m_{\alpha\text{-KG}} = 26.0$ ($n = 71$), $P < 0.0001$; or N2, $m_{\text{veh}} = 21.5$ ($n = 101$), $m_{\alpha\text{-KG}} = 24.6$ ($n = 102$), $P < 0.0001$. P values were determined by the log-rank test. Number of independent experiments: RNAi control (6), *atp-2* (2), *let-363* (3), N2 (5), *daf-2* (2), *pha-4* (2), *daf-16* (2), *hif-1* (5).

α -KG. This requirement is specific because, in contrast, the lifespan of the even longer-lived insulin/IGF-1 receptor *daf-2(e1370)* mutant worms³ is further increased by α -KG (Fig. 3b). Remarkably, oligomycin, an inhibitor of ATP synthase, also extends the lifespan of adult worms (Extended Data Fig. 3a). Together, the direct binding of ATP-2 by α -KG, the related enzymatic inhibition, reduction in ATP levels and oxygen consumption, lifespan analysis, and other similarities (see also Supplementary Notes, Extended Data Fig. 4) to *atp-2* knockdown or oligomycin treatment demonstrate that α -KG probably extends lifespan primarily by targeting ATP-2.

The lower ATP content in α -KG-treated animals suggests that increased longevity by α -KG may involve a state similar to that induced by dietary restriction. Consistent with this idea, we found that α -KG does not extend the lifespan of *eat-2(ad1116)* animals (Fig. 3c), which is a model of dietary restriction with impaired pharyngeal pumping and therefore reduced food intake¹⁶. The longevity of *eat-2* mutants requires TOR (encoded by the *C. elegans* orthologue *let-363*)¹⁷, an important mediator of the effects of dietary restriction on longevity¹⁸. Likewise, α -KG fails to increase the lifespan of *let-363* RNAi animals (Fig. 3d). The AMP-activated protein kinase (AMPK) is another conserved major sensor of cellular energy status¹⁹. Both AMPK (*C. elegans* orthologue *aak-2*) and the FoxO transcription factor DAF-16 mediate dietary-restriction-induced longevity in *C. elegans* fed diluted bacteria²⁰, but neither is required for lifespan extension in the *eat-2* model^{16,20}. We found that in *aak-2* (Extended Data Fig. 5a) and *daf-16* (Fig. 3e) mutants the longevity effect of α -KG is smaller than in N2 animals ($P < 0.0001$), suggesting that α -KG longevity partially depends on AMPK and FoxO; nonetheless, lifespan is significantly increased by α -KG in *aak-2* (24.3%, $P < 0.0001$) and *daf-16* (29.5%, $P < 0.0001$) mutant or RNAi animals (Fig. 3e and Extended Data Fig. 5a, b; data not shown), indicating an AMPK- and FoxO-independent effect of α -KG in increasing longevity.

The inability of α -KG to extend further the lifespan of *let-363* RNAi animals suggests that α -KG treatment and TOR inactivation extend lifespan either through the same pathway (with α -KG acting on or upstream of TOR), or through independent mechanisms or parallel pathways that converge on a downstream effector. The first model predicts that the

TOR pathway will be less active upon α -KG treatment, whereas if the latter model were true then TOR would be unaffected by α -KG treatment. In support of the first model, we found that TOR pathway activity is decreased in human cells treated with octyl α -KG (Fig. 4a and Extended Data Fig. 6a, b). However, α -KG does not interact with TOR directly (Extended Data Fig. 6d, e). Consistent with the involvement of TOR in α -KG longevity, the FoxA transcription factor PHA-4, which is required to extend adult lifespan in response to reduced TOR signalling²¹ and for dietary-restriction-induced longevity in *C. elegans*²², is likewise required for α -KG-induced longevity (Fig. 3f). Moreover, autophagy, which is activated both by TOR inhibition^{18,23} and by dietary restriction²⁴, is markedly increased in worms treated with α -KG (or *ogdh-1* RNAi) and in *atp-2* RNAi animals (Fig. 4b, c, Extended Data Figs 6c, 7 and Supplementary Notes), as indicated by the prevalence of green fluorescent protein GFP::LGG-1 puncta (Methods). Autophagy was also induced in mammalian cells treated with octyl α -KG (Extended Data Fig. 6f). Furthermore, α -KG does not result in significantly more autophagy in either *atp-2* RNAi or *let-363* RNAi worms (Fig. 4b, c). The data provide further evidence that α -KG decreases TOR pathway activity through the inhibition of ATP synthase. Similarly, autophagy is induced by oligomycin, and oligomycin does not augment autophagy in *let-363* RNAi worms (Extended Data Fig. 3b, c).

α -KG is not only a metabolite, but also a co-substrate for a large family of dioxygenases²⁵. The hypoxia inducible factor (HIF-1) is modified by one of these enzymes, the prolyl 4-hydroxylase (PHD) EGL-9, and thereafter degraded by the von Hippel-Lindau (VHL) protein^{26,27}. α -KG extends the lifespan of animals with loss-of-function mutations in *hif-1*, *egl-9* and *vhl-1* (Fig. 3g and Extended Data Fig. 5c), suggesting that this pathway does not play a major part in lifespan extension by α -KG. However, it is prudent to acknowledge that the formal possibility of other α -KG-binding targets having an additional role in the extension of lifespan by α -KG cannot be eliminated at this time.

We show that ageing in *C. elegans* is delayed by α -KG supplementation in adult animals. This longevity effect is probably mediated by ATP synthase, which we identified as a direct target of α -KG, and TOR, a major effector of dietary restriction. Identification of new protein targets

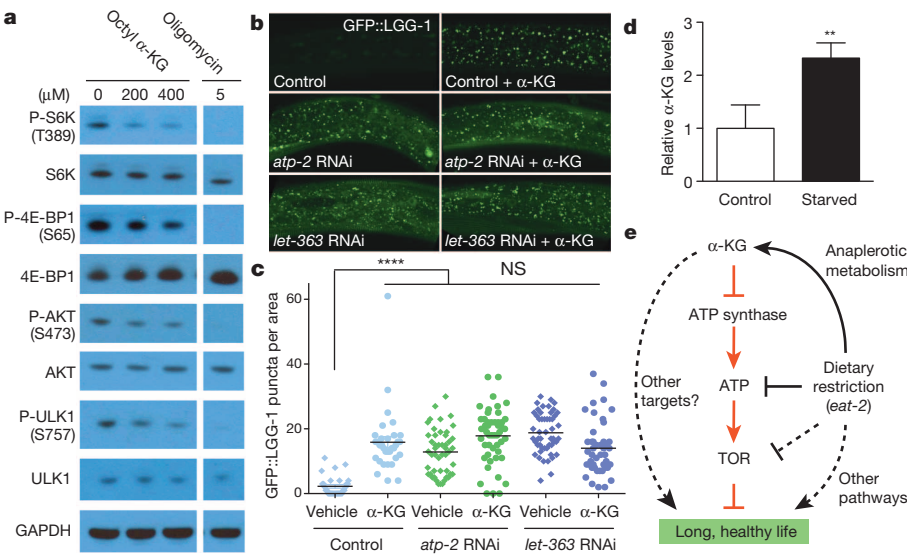


Figure 4 | Inhibition of ATP synthase by α -KG causes a conserved decrease in TOR pathway activity. **a**, Decreased phosphorylation of mammalian TOR substrates in U87 cells treated with octyl α -KG or oligomycin. Similar results were obtained in HEK-293 cells, normal human fibroblasts and mouse embryonic fibroblasts (data not shown). P, phospho. **b**, Increased autophagy in animals treated with α -KG or RNAi for *atp-2* or *let-363*. Photographs were

taken at $\times 100$ magnification. **c**, GFP::LGG-1 puncta quantified using ImageJ (Methods). Data show results of 2–3 independent experiments. Bars indicate the mean. **** $P < 0.0001$; NS, not significant (*t*-test, two-tailed, two-sample unequal variance). **d**, α -KG levels are increased in starved worms. ** $P < 0.01$ (*t*-test, two-tailed, two-sample unequal variance). Mean \pm s.d. is plotted. **e**, Model of α -KG-mediated longevity.

taken at $\times 100$ magnification. **c**, GFP::LGG-1 puncta quantified using ImageJ (Methods). Data show results of 2–3 independent experiments. Bars indicate the mean. **** $P < 0.0001$; NS, not significant (*t*-test, two-tailed, two-sample unequal variance). **d**, α -KG levels are increased in starved worms. ** $P < 0.01$ (*t*-test, two-tailed, two-sample unequal variance). Mean \pm s.d. is plotted. **e**, Model of α -KG-mediated longevity.

Online Content Any additional Methods, Extended Data display items and Source Data are available in the online version of the paper; references unique to these sections appear only in the online paper.

Received 3 October 2012; accepted 17 March 2014.

Published online 14 May 2014.

- Colman, R. J. *et al.* Caloric restriction delays disease onset and mortality in rhesus monkeys. *Science* **325**, 201–204 (2009).
- Mattison, J. A. *et al.* Impact of caloric restriction on health and survival in rhesus monkeys from the NIA study. *Nature* **489**, 318–321 (2012).
- Kenyon, C. J. The genetics of ageing. *Nature* **464**, 504–512 (2010).
- Harrison, D. E. *et al.* Rapamycin fed late in life extends lifespan in genetically heterogeneous mice. *Nature* **460**, 392–395 (2009).
- Williams, D. S., Cash, A., Hamadani, L. & Diemer, T. Oxaloacetate supplementation increases lifespan in *Caenorhabditis elegans* through an AMPK/FOXO-dependent pathway. *Aging Cell* **8**, 765–768 (2009).
- Lucanic, M. *et al.* N-acylethanolamine signalling mediates the effect of diet on lifespan in *Caenorhabditis elegans*. *Nature* **473**, 226–229 (2011).
- Lomenick, B. *et al.* Target identification using drug affinity responsive target stability (DARTS). *Proc. Natl Acad. Sci. USA* **106**, 21984–21989 (2009).
- Abrahams, J. P., Leslie, A. G., Lutter, R. & Walker, J. E. Structure at 2.8 Å resolution of F1-ATPase from bovine heart mitochondria. *Nature* **370**, 621–628 (1994).
- Boyer, P. D. The ATP synthase—a splendid molecular machine. *Annu. Rev. Biochem.* **66**, 717–749 (1997).
- Tsang, W. Y., Sayles, L. C., Grad, L. I., Pilgrim, D. B. & Lemire, B. D. Mitochondrial respiratory chain deficiency in *Caenorhabditis elegans* results in developmental arrest and increased life span. *J. Biol. Chem.* **276**, 32240–32246 (2001).
- Dillin, A. *et al.* Rates of behavior and aging specified by mitochondrial function during development. *Science* **298**, 2398–2401 (2002).
- Lee, S. S. *et al.* A systematic RNAi screen identifies a critical role for mitochondria in *C. elegans* longevity. *Nature Genet.* **33**, 40–48 (2002).
- Curran, S. P. & Ruvkun, G. Lifespan regulation by evolutionarily conserved genes essential for viability. *PLoS Genet.* **3**, e56 (2007).
- Gems, D. & Riddle, D. L. Genetic, behavioral and environmental determinants of male longevity in *Caenorhabditis elegans*. *Genetics* **154**, 1597–1610 (2000).
- Brand, M. D. & Nicholls, D. G. Assessing mitochondrial dysfunction in cells. *Biochem. J.* **435**, 297–312 (2011).
- Lakowski, B. & Hekimi, S. The genetics of caloric restriction in *Caenorhabditis elegans*. *Proc. Natl Acad. Sci. USA* **95**, 13091–13096 (1998).
- Hansen, M. *et al.* Lifespan extension by conditions that inhibit translation in *Caenorhabditis elegans*. *Aging Cell* **6**, 95–110 (2007).
- Stanfel, M. N., Shamieh, L. S., Kaeberlein, M. & Kennedy, B. K. The TOR pathway comes of age. *Biochim. Biophys. Acta* **1790**, 1067–1074 (2009).
- Hardie, D. G., Scott, J. W., Pan, D. A. & Hudson, E. R. Management of cellular energy by the AMP-activated protein kinase system. *FEBS Lett.* **546**, 113–120 (2003).

20. Greer, E. L. & Brunet, A. Different dietary restriction regimens extend lifespan by both independent and overlapping genetic pathways in *C. elegans*. *Aging Cell* **8**, 113–127 (2009).
21. Sheaffer, K. L., Updike, D. L. & Mango, S. E. The target of rapamycin pathway antagonizes *pha-4*/FoxA to control development and aging. *Curr. Biol.* **18**, 1355–1364 (2008).
22. Panowski, S. H., Wolff, S., Aguilaniu, H., Durieux, J. & Dillin, A. PHA-4/FoxA mediates diet-restriction-induced longevity of *C. elegans*. *Nature* **447**, 550–555 (2007).
23. Wullschleger, S., Loewith, R. & Hall, M. N. TOR signaling in growth and metabolism. *Cell* **124**, 471–484 (2006).
24. Meléndez, A. et al. Autophagy genes are essential for dauer development and life-span extension in *C. elegans*. *Science* **301**, 1387–1391 (2003).
25. Loenarz, C. & Schofield, C. J. Expanding chemical biology of 2-oxoglutarate oxygenases. *Nature Chem. Biol.* **4**, 152–156 (2008).
26. Epstein, A. C. et al. *C. elegans* EGL-9 and mammalian homologs define a family of dioxygenases that regulate HIF by prolyl hydroxylation. *Cell* **107**, 43–54 (2001).
27. Zhang, Y., Shao, Z., Zhai, Z., Shen, C. & Powell-Coffman, J. A. The HIF-1 hypoxia-inducible factor modulates lifespan in *C. elegans*. *PLoS ONE* **4**, e6348 (2009).
28. Brauer, M. J. et al. Conservation of the metabolomic response to starvation across two divergent microbes. *Proc. Natl Acad. Sci. USA* **103**, 19302–19307 (2006).
29. Kaminsky, Y. G., Kosenko, E. A. & Kondrashova, M. N. Metabolites of citric acid cycle, carbohydrate and phosphorus metabolism, and related reactions, redox and phosphorylating states of hepatic tissue, liver mitochondria and cytosol of the pigeon, under normal feeding and natural nocturnal fasting conditions. *Comp. Biochem. Physiol. B* **73**, 957–963 (1982).
30. Brugnara, L. et al. Metabolomics approach for analyzing the effects of exercise in subjects with type 1 diabetes mellitus. *PLoS ONE* **7**, e40600 (2012).

Supplementary Information is available in the online version of the paper.

Acknowledgements We thank S. Lee, M. Hansen, B. Lemire, A. van der Bliek, S. Clarke, T. K. Blackwell, R. Johnson, J. E. Walker, A. G. W. Leslie, K. N. Houk, B. Martin, J. Lusis, J. Gober, Y. Wang and H. Sun for advice and discussions. J. Avruch for the *let-363* RNAi vector; J. Powell-Coffman for strains and advice; and K. Yan for technical assistance. Worm strains were provided by the *Caenorhabditis* Genetics Center, which is funded by the National Institutes of Health (NIH) Office of Research Infrastructure Programs (P40 OD010440). We thank the NIH for traineeship support of R.M.C. (T32 GM007104), M.Y.P. (T32 GM007185), B.L. (T32 GM008496) and M.N. (T32 CA009120). X.F. is a recipient of the China Scholarship Council Scholarship. G.C.M. was supported by Ford Foundation and National Science Foundation Graduate Research Fellowships.

Author Contributions Lifespan assays were performed by R.M.C., M.P. and E.H.; DARTS-mass spectrometry by S.D. and B.L.; DARTS-western blots by M.Y.P., H.H. and R.M.C.; mammalian cell experiments by X.F. and H.H.; mitochondrial respiration study design and analyses by L.V. and K.R.; enzyme kinetics and analyses by R.M.C. and J.H.; confocal microscopy by V.S.M., G.C.M. and A.R.F.; ultra-high-performance liquid chromatography-electrospray ionization-tandem mass spectrometry (UHPLC-ESI/MS/MS) by J.X.W. and S.A.T.; compound syntheses by G.D. and M.E.J.; other analyses by H.H., X.F., M.Y.P., D.B., R.M.C., E.H., G.J., G.M.S., C.K. and A.Q. S.A.W., F.F., M.N., A.S.K., H.A.G., H.R. Chang, K.F.F., F.G., M.J., S.A.T., A.S., D.B., H.R. Christofk, C.F.C., M.A.T., M.E.J., L.V., K.R., A.R.F. and M.P. provided guidance, specialized reagents and expertise. J.H. conceived the study. R.M.C. and J.H. wrote the paper. R.M.C., X.F. and J.H. analysed data. All authors discussed the results, commented on the studies and contributed to aspects of preparing the manuscript.

Author Information Reprints and permissions information is available at www.nature.com/reprints. The authors declare no competing financial interests. Readers are welcome to comment on the online version of the paper. Correspondence and requests for materials should be addressed to J.H. (jinghuang@mednet.ucla.edu).

METHODS

Nematode strains and maintenance. *C. elegans* strains were maintained using standard methods³¹. The following strains were used (strain, genotype): Bristol N2, wild type; DA1116, eat-2(ad1116)II; CB1370, daf-2(e1370)III; CF1038, daf-16(mu86)I; PD8120, smg-1(cc546ts)I; SM190, smg-1(cc546ts)I; pha-4(zu225)V; RB754, aak-2(ok524)X; ZG31, hif-1(iia4)V; ZG596, hif-1(iia7)V; JT307, egl-9(sa307)V; CB5602, vhl-1(ok161)X; DA2123, adls2122[lgg-1::GFP + rol-6(su1006)]. They were all obtained from the *Caenorhabditis* Genetics Center (CGC).

RNAi in *C. elegans*. RNAi in *C. elegans* was accomplished by feeding worms HT115 (DE3) bacteria expressing target-gene double-stranded RNA (dsRNA) from the pL4440 vector³². dsRNA production was induced overnight on plates containing 1 mM isopropyl-β-D-thiogalactoside (IPTG). All RNAi feeding clones were obtained from the *C. elegans* ORF-RNAi Library (Thermo Scientific/Open Biosystems) unless otherwise stated. The *C. elegans* TOR (*let-363*) RNAi clone³³ was obtained from Joseph Avruch (MGH/Harvard). Efficient knockdown was confirmed by western blotting of the corresponding protein or by qRT-PCR of the mRNA. The primer sequences used for qRT-PCR are as follows. *atp-2* forward: TGACAAACATTITTC CGTTTCACT; *atp-2* reverse: AAATAGCCTGGACGGATGTGAT; *let-363* forward: GATCCGAGACAAGATGAACGT; *let-363* reverse: ACAATTGGAAC CCAACCAATC; *ogdh-1* forward: TGATTGGACCGAGAATTCCTT; *ogdh-1* reverse: GGATCAGACGTTGAAACAGCAC.

We validated the RNAi knockdown of both *ogdh-1* and *atp-2* by quantitative RT-PCR and also of *atp-2* by western blotting. Transcripts of *ogdh-1* were reduced by 85%, and transcripts and protein levels of *atp-2* were reduced by 52% and 83%, respectively, in larvae that were cultivated on bacteria that expressed the corresponding dsRNAs. In addition, RNAi of *atp-2* in this study was associated with delayed post-embryonic development and larval arrest, consistent with the phenotypes of *atp-2(ua2)* animals. Analysis by qRT-PCR indicated a modest but significant decrease by 26% in transcripts of *let-363* in larvae undergoing RNAi; moreover, molecular markers for autophagy were induced in these animals, and the lifespan of adults was extended, consistent with partial inactivation of the kinase.

In lifespan experiments, we used RNAi to inactivate *atp-2*, *ogdh-1* and *let-363* in mature animals in the presence or absence of exogenous α-KG. The concentration of α-KG used in these experiments (8 mM) was empirically determined to be most beneficial for wild-type animals (Fig. 1c). This approach enabled us to evaluate the contribution of essential proteins and pathways to the longevity conferred by supplementary α-KG. Specifically, we were able to substantially but not fully inactivate *atp-2* in adult animals that had completed embryonic and larval development. As described earlier, supplementation with 8 mM α-KG did not further extend (and in fact, on one occasion, even decreased) the lifespan of *atp-2* RNAi animals (Extended Data Table 2), indicating that *atp-2* is required for α-KG to promote longevity. On the other hand, a complete inactivation of *atp-2* would be lethal, and thereby mask the benefit of ATP synthase inhibition by α-KG.

Lifespan analysis. Lifespan assays were conducted at 20 °C on solid nematode growth media (NGM) using standard protocols and were replicated in at least two independent experiments. *C. elegans* were synchronized by performing either a timed egg lay³⁴ or an egg preparation (lysing ~100 gravid worms in 70 μl M9 buffer³¹, 25 μl bleach (10% sodium hypochlorite solution) and 5 μl 10 N NaOH). Young adult animals were picked onto NGM assay plates containing 1.5% dimethyl sulfoxide (DMSO; Sigma, D8418), 49.5 μM 5-fluoro-2'-deoxyuridine³⁴ (FUDR; Sigma, F0503), and α-KG (Sigma, K1128) or vehicle control (H₂O). FUDR was included to prevent progeny production. Media containing α-KG were adjusted to pH 6.0 (that is, the same pH as the control plates) by the addition of NaOH. All compounds were mixed into the NGM media after autoclaving and before solidification of the media. Assay plates were seeded with OP50 (or a designated RNAi feeding clone, see later). Worms were moved to new assay plates every 4 days (to ensure sufficient food was present at all times and to reduce the risk of mould contamination). To assess the survival of the worms, the animals were prodded with a platinum wire every 2–3 days, and those that failed to respond were scored as dead. For analysis concerning mutant strains, the corresponding parent strain was used as a control in the same experiment.

For lifespan experiments involving RNAi, the plates also contained 1 mM IPTG (Acros, CAS 367-93-1) and 50 μg ml⁻¹ ampicillin (Fisher, BP1760-25). RNAi was accomplished by feeding N2 worms HT115(DE3) bacteria expressing target-gene dsRNA from pL4440 (ref. 32); control RNAi was done in parallel for every experiment by feeding N2 worms HT115(DE3) bacteria expressing either GFP dsRNA or empty vector (which gave identical lifespan results).

Lifespan experiments with oligomycin (Cell Signaling, 9996) were performed as described for α-KG (that is, NGM plates with 1.5% DMSO and 49.5 μM FUDR; N2 worms; OP50 bacteria).

For lifespan experiments concerning *smg-1(cc546ts);pha-4(zu225)* and *smg-1(cc546ts)*^{32,35}, from egg to L4 stage the strains were grown at 24 °C, which inactivates the *smg-1* temperature-sensitive allele, preventing mRNA surveillance-mediated degradation of the *pha-4(zu225)* mRNA, which contains a premature stop codon,

and thus produces a truncated but fully functional PHA-4 transcription factor³⁵. Then at the L4 stage the temperature was shifted to 20 °C, which restores *smg-1* function and thereby results in the degradation of *pha-4(zu225)* mRNA. Treatment with α-KG began at the L4 stage.

All lifespan data are available in Extended Data Table 2, including sample sizes. The sample size was chosen on the basis of standards done in the field in published manuscripts. No statistical method was used to predetermine the sample size. Animals were assigned randomly to the experimental groups. Worms that ruptured, bagged (that is, exhibited internal progeny hatching), or crawled off the plates were censored. Lifespan data were analysed using GraphPad Prism; P values were calculated using the log-rank (Mantel-Cox) test.

Statistical analyses. All experiments were repeated at least two times with identical or similar results. Data represent biological replicates. Appropriate statistical tests were used for every figure. Data meet the assumptions of the statistical tests described for each figure. Mean ± s.d. is plotted in all figures unless stated otherwise.

Food preference assay. Protocol adapted from Abada *et al.*³⁶. A 10 cm NGM plate was seeded with two spots of OP50 as shown in Extended Data Fig. 1e. After letting the OP50 lawns dry over 2 days at room temperature, vehicle (H₂O) or α-KG (8 mM) was added to the top of the lawn and allowed to dry over 2 days at room temperature. Approximately 50–100 synchronized adult day 1 worms were placed onto the centre of the plate and their preference for either bacterial lawn was recorded after 3 h at room temperature.

Target identification using DARTS. For unbiased target identification (Fig. 2a), human Jurkat cells were lysed using M-PER (Thermo Scientific, 78501) with the addition of protease inhibitors (Roche, 11836153001) and phosphatase inhibitors³⁷. TNC buffer (50 mM Tris-HCl pH 8.0, 50 mM NaCl, 10 mM CaCl₂) was added to the lysate and protein concentration was then determined using the BCA Protein Assay kit (Pierce, 23227). Cell lysates were incubated with either vehicle (H₂O) or α-KG for 1 h on ice followed by an additional 20 min at room temperature. Digestion was performed using Pronase (Roche, 10165921001) at room temperature for 30 min and stopped using excess protease inhibitors with immediate transfer to ice. The resulting digests were separated by SDS-PAGE and visualized using SYPRO Ruby Protein Gel Stain (Invitrogen, S12000). The band with increased staining from the α-KG lane (corresponding to potential protein targets that are protected from proteolysis by the binding of α-KG) and the matching area of the control lane were excised, in-gel trypsin digested, and subjected to liquid chromatography-tandem mass spectrometry (LC-MS/MS) analysis as described previously^{7,38}. Mass spectrometry results were searched against the human Swissprot database (release 57.15) using Mascot version 2.3.0, with all peptides meeting a significance threshold of P < 0.05.

For target verification by DARTS with western blotting (Fig. 2b), HeLa cells were lysed in M-PER buffer (Thermo Scientific, 78501) with the addition of protease inhibitors (Roche, 11836153001) and phosphatase inhibitors (50 mM NaF, 10 mM β-glycerophosphate, 5 mM sodium pyrophosphate, 2 mM Na₃VO₄). Chilled TNC buffer (50 mM Tris-HCl pH 8.0, 50 mM NaCl, 10 mM CaCl₂) was added to the protein lysate, and protein concentration of the lysate was measured by the BCA Protein Assay kit (Pierce, 23227). The protein lysate was then incubated with vehicle control (H₂O) or varying concentrations of α-KG for 3 h at room temperature with shaking at 600 r.p.m. in an Eppendorf Thermomixer. Pronase (Roche, 10165921001) digestions were performed for 20 min at room temperature, and stopped by adding SDS loading buffer and immediately heating at 70 °C for 10 min. Samples were subjected to SDS-PAGE on 4–12% Bis-Tris gradient gel (Invitrogen, NP0322BOX) and western blotted for ATP synthase subunits ATP5B (Sigma, AV48185), ATP5O (Abcam, ab91400) and ATP5A (Abcam, ab110273). Binding between α-KG and PHD-2 (encoded by EGLN1) (Cell Signaling, 4835), for which α-KG is a co-substrate³⁹, was confirmed by DARTS. GAPDH (Ambion, AM4300) was used as a negative control.

For DARTS using *C. elegans* (Extended Data Fig. 2a), wild-type animals of various ages were grown on NGM/OP50 plates, washed four times with M9 buffer, and immediately placed in the -80 °C freezer. Animals were lysed in HEPES buffer (40 mM HEPES pH 8.0, 120 mM NaCl, 10% glycerol, 0.5% Triton X-100, 10 mM β-glycerophosphate, 50 mM NaF, 0.2 mM Na₃VO₄, protease inhibitors (Roche, 11836153001)) using Lysing Matrix C tubes (MP Biomedicals, 6912-100) and the FastPrep-24 (MP Biomedicals) high-speed bench-top homogenizer in the 4 °C room (disrupt worms for 20 s at 6.5 m s⁻¹, rest on ice for 1 min; repeat twice). Lysed animals were centrifuged at 14,000 r.p.m. for 10 min at 4 °C to pellet worm debris, and supernatant was collected for DARTS. Protein concentration was determined by BCA Protein Assay kit (Pierce, 23223). A worm lysate concentration of 1.13 μg μl⁻¹ was used for the DARTS experiment. All steps were performed on ice or at 4 °C to help prevent premature protein degradation. TNC buffer (50 mM Tris-HCl pH 8.0, 50 mM NaCl, 10 mM CaCl₂) was added to the worm lysates. Worm lysates were incubated with vehicle control (H₂O) or α-KG for 1 h on ice and then 50 min at room temperature. Pronase (Roche, 10165921001) digestions were performed for

30 min at room temperature and stopped by adding SDS loading buffer and heating at 70 °C for 10 min. Samples were then subjected to SDS-PAGE on NuPAGE Novex 4–12% Bis-Tris gradient gels (Invitrogen, NP0322BOX), and western blotting was carried out with an antibody against ATP5B (Sigma, AV48185) that also recognizes ATP-2.

Complex V activity assay. Complex V activity was assayed using the MitoTox OXPHOS Complex V Activity Kit (Abcam, ab109907). Vehicle (H_2O) or α -KG was mixed with the enzyme before the addition of phospholipids. In experiments using octyl α -KG, vehicle (1% DMSO) or octyl α -KG was added with the phospholipids. Relative complex V activity was compared to vehicle. Oligomycin (Sigma, O4876) was used as a positive control for the assay.

Isolation of mitochondria from mouse liver. Animal studies were performed under approved University of California, Los Angeles animal research protocols. Mitochondria from 3-month-old C57BL/6 mice were isolated as described⁴⁰. Briefly, livers were extracted, minced at 4 °C in MSHE plus BSA (70 mM sucrose, 210 mM mannitol, 5 mM HEPES, 1 mM EGTA, and 0.5% fatty acid free BSA, pH 7.2), and rinsed several times to remove blood. All subsequent steps were performed on ice or at 4 °C. The tissue was disrupted in ten volumes of MSHE plus BSA with a glass Dounce homogenizer (5–6 strokes) and the homogenate was centrifuged at 800g for 10 min to remove tissue debris and nuclei. The supernatant was decanted through a cell strainer and centrifuged at 8,000g for 10 min. The dark mitochondrial pellet was resuspended in MSHE plus BSA and re-centrifuged at 8,000g for 10 min. The final mitochondrial pellets were used for various assays as described later.

Submitochondrial particle ATPase assay. ATP hydrolysis by ATP synthase was measured using submitochondrial particles (see ref. 41 and references therein). Mitochondria were isolated from mouse liver as described earlier. The final mitochondrial pellet was resuspended in buffer A (250 mM sucrose, 10 mM Tris-HCl, 1 mM ATP, 5 mM MgCl₂ and 0.1 mM EGTA, pH 7.4) at 10 μ g μ l⁻¹, subjected to sonication on ice (Fisher Scientific Model 550 Sonic Dismembrator; medium power, alternating between 10 s intervals of sonication and resting on ice for a total of 60 s of sonication), and then centrifuged at 18,000g for 10 min at 4 °C. The supernatant was collected and centrifuged at 100,000g for 45 min at 4 °C. The final pellet (submitochondrial particles) was resuspended in buffer B (250 mM sucrose, 10 mM Tris-HCl and 0.02 mM EGTA, pH 7.4).

The SMP ATPase activity was assayed using the Complex V Activity Buffer as described earlier. The production of ADP is coupled to the oxidation of NADH to NAD⁺ through pyruvate kinase and lactate dehydrogenase. The addition of α -KG (up to 10 mM) did not affect the activity of pyruvate kinase or lactate dehydrogenase when external ADP was added. The absorbance decrease of NADH at 340 nm correlates to ATPase activity. Submitochondrial particles (2.18 ng μ l⁻¹) were incubated with vehicle or α -KG for 90 min at room temperature before the addition of activity buffer, and then the absorbance decrease of NADH at 340 nm was measured every 1 min for 1 h. Oligomycin (Cell signaling, 9996) was used as a positive control for the assay.

Assay for ATP levels. Normal human diploid fibroblast WI-38 (ATCC, CCL-75) cells were seeded in 96-well plates at 2 × 10⁴ cells per well. Cells were treated with either DMSO (vehicle control) or octyl α -KG at varying concentrations for 2 h in triplicate. ATP levels were measured using the CellTiter-Glo luminescent ATP assay (Promega, G7572); luminescence was read using Analyst HT (Molecular Devices). In parallel, identically treated cells were lysed in M-PER (Thermo Scientific, 78501) to obtain protein concentration by BCA Protein Assay kit (Pierce, 23223). ATP levels were normalized to protein content. Statistical analysis was performed using GraphPad Prism (unpaired *t*-test).

The assay for ATP levels in *C. elegans* was carried out as follows. Synchronized day 1 adult wild-type *C. elegans* were placed on NGM plates containing either vehicle or 8 mM α -KG. On day 2 and 8 of adulthood, 9 replicates and 4 replicates, respectively, of about 100 worms were collected from α -KG or vehicle control plates, washed 4 times in M9 buffer, and frozen in –80 °C. Animals were lysed using Lysing Matrix C tubes (MP Biomedicals, 6912-100) and the FastPrep-24 (MP Biomedicals) high-speed bench-top homogenizer (disrupt worms for 20 s at 6.5 m s⁻¹, rest on ice for 1 min; repeat twice). Lysed animals were centrifuged at 14,000 r.p.m. for 10 min at 4 °C to pellet worm debris, and supernatant was saved for ATP quantification using the Kinase-Glo Luminescent Kinase Assay Platform (Promega, V6713) according to the manufacturer's instructions. The assay was performed in white opaque 96-well tissue culture plates (Falcon, 353296), and luminescence was measured using Analyst HT (Molecular Devices). ATP levels were normalized to the number of worms. Statistical analysis was performed using Microsoft Excel (*t*-test, two-tailed, two-sample unequal variance).

Measurement of oxygen consumption rates. Oxygen consumption rate (OCR) measurements were made using a Seahorse XF-24 analyser (Seahorse Bioscience)⁴². Cells were seeded in Seahorse XF-24 cell culture microplates at 50,000 cells per well in DMEM media supplemented with 10% FBS and 10 mM glucose, and incubated at 37 °C and 5% CO₂ overnight. Treatment with octyl α -KG or DMSO (vehicle control)

was for 1 h. Cells were washed in unbuffered DMEM medium (pH 7.4, 10 mM glucose) just before measurement, and maintained in this buffer with indicated concentrations of octyl α -KG. OCR was measured three times under basal conditions and normalized to protein concentration per well. Statistical analysis was performed using GraphPad Prism.

Measurement of OCR in living *C. elegans* was carried out as follows. The protocol was adapted from those previously described^{43,44}. Wild-type day 1 adult N2 worms were placed on NGM plates containing 8 mM α -KG or H_2O (vehicle control) seeded with OP50 or HT115 *E. coli*. OCR was assessed on day 2 of adulthood. On day 2 of adulthood, worms were collected and washed four times with M9 to rid the samples of bacteria (we further verified that α -KG does not affect oxygen consumption of the bacteria—therefore, even if there were any leftover bacteria after the washes, the changes in OCR observed would still be worm specific), and then the animals were seeded in quadruplicates in Seahorse XF-24 cell culture microplates (Seahorse Bioscience, V7-PS) in 200 μ l M9 at ~200 worms per well. Oxygen consumption rates were measured seven times under basal conditions and normalized to the number of worms counted per well. The experiment was repeated twice. Statistical analysis was performed using Microsoft Excel (*t*-test, two-tailed, two-sample unequal variance).

Measurement of mitochondrial respiratory control ratio. Mitochondrial respiratory control ratio (RCR) was analysed using isolated mouse liver mitochondria (see ref. 15 and references therein). Mitochondria were isolated from mouse liver as described earlier. The final mitochondrial pellet was resuspended in 30 μ l of MAS buffer (70 mM sucrose, 220 mM mannitol, 10 mM KH₂PO₄, 5 mM MgCl₂, 2 mM HEPES, 1 mM EGTA, and 0.2% fatty acid free BSA, pH 7.2).

Isolated mitochondrial respiration was measured by running coupling and electron flow assays as described⁴⁰. For the coupling assay, 20 μ g of mitochondria in complete MAS buffer (MAS buffer supplemented with 10 mM succinate and 2 μ M rotenone) were seeded into a XF24 Seahorse plate by centrifugation at 2,000g for 20 min at 4 °C. Just before the assay, the mitochondria were supplemented with complete MAS buffer for a total of 500 μ l (with 1% DMSO or octyl α -KG), and warmed at 37 °C for 30 min before starting the OCR measurements. Mitochondrial respiration begins in a coupled state 2; state 3 is initiated by 2 mM ADP; state 4o (oligomycin insensitive, that is, complex V independent) is induced by 2.5 μ M oligomycin; and state 3u (FCCP-uncoupled maximal respiratory capacity) by 4 μ M FCCP. Finally, 1.5 μ g ml⁻¹ antimycin A was injected at the end of the assay. The state 3/state 4o ratio gives the RCR.

For the electron flow assay, the MAS buffer was supplemented with 10 mM sodium pyruvate (complex I substrate), 2 mM malate (complex II inhibitor) and 4 μ M FCCP, and the mitochondria are seeded the same way as described for the coupling assay. After basal readings, the sequential injections were as follows: 2 μ M rotenone (complex I inhibitor), 10 mM succinate (complex II substrate), 4 μ M antimycin A (complex III inhibitor) and 10 mM/100 μ M ascorbate/tetramethylphenylenediamine (complex IV substrate).

ATP synthase enzyme inhibition kinetics. ATP synthesis enzyme inhibition kinetic analysis was performed using isolated mitochondria. Mitochondria were isolated from mouse liver as described earlier. The final mitochondrial pellet was resuspended in MAS buffer supplemented with 5 mM sodium ascorbate (Sigma, A7631) and 5 mM TMPD (Sigma, T7394).

The reaction was carried out in MAS buffer containing 5 mM sodium ascorbate, 5 mM TMPD, luciferase reagent (Roche, 11699695001), octanol or octyl α -KG, variable amounts of ADP (Sigma, A2754), and 3.75 ng μ l⁻¹ mitochondria. ATP synthesis was monitored by the increase in luminescence over time by a luminometer (Analyst HT, Molecular Devices). ATP-synthase-independent ATP formation, derived from the oligomycin-insensitive luminescence, was subtracted as background. The initial velocity of ATP synthesis was calculated from the slope of the first 3 min of the reaction, before the velocity begins to decrease. Enzyme inhibition kinetics was analysed by nonlinear regression least-squares fit using GraphPad Prism.

Assay for mammalian TOR pathway activity. Mammalian (m)TOR pathway activity in cells treated with octyl α -KG or oligomycin was determined by the levels of phosphorylation of known mTOR substrates, including S6K (T389), 4E-BP1 (S65), AKT (S473) and ULK1 (S757)^{45–49}. Specific antibodies used: phospho (P)-S6K T389 (Cell Signaling, 9234), S6K (Cell Signaling, 9202S), P-4E-BP1 S65 (Cell Signaling, 9451S), 4E-BP1 (Cell Signaling, 9452S), P-AKT S473 (Cell Signaling, 4060S), AKT (Cell Signaling, 4691S), P-ULK1 S757 (Cell Signaling, 6888), ULK1 (Cell Signaling, 4773S) and GAPDH (Santa Cruz Biotechnology, 25778).

Assay for autophagy. DA2123 animals carrying an integrated GFP::LGG-1 translational fusion gene^{50–52}, were used to quantify levels of autophagy. To obtain a synchronized population of DA2123, we performed an egg preparation of gravid adults (by lysing ~100 gravid worms in 70 μ l M9 buffer, 25 μ l bleach and 5 μ l 10 N NaOH) and allowed the eggs to hatch overnight in M9, causing starvation-induced L1 diapause. L1 larvae were deposited onto NGM treatment plates containing vehicle,

8 mM α -KG or 40 μ M oligomycin, and seeded with either *E. coli* OP50, HT115(DE3) with an empty vector, or HT115(DE3)-expressing dsRNAs targeting *atp-2*, *let-363* or *ogdh-1* as indicated. When the majority of animals in a given sample first reached the mid-L3 stage, individual L3 larvae were mounted onto microscope slides and anaesthetized with 1.6 mM levamisole (Sigma, 31742). Nematodes were observed using an Axiovert 200M Zeiss confocal microscope with a LSM5 Pascal laser, and images were captured using the LSM Image Examiner (Zeiss). For each specimen, GFP::LGG-1 puncta (autophagosomes) in the epidermis, including the lateral seam cells and Hyp7, were counted in three separate regions of $140.97 \mu\text{m}^2$ using ‘analyze particles’ in ImageJ⁵³. Measurements were made blind to both the genotype and supplement. Statistical analysis was performed using Microsoft Excel (*t*-test, two-tailed, two-sample unequal variance).

The assay for autophagy in mammalian cells was carried out as follows. HEK-293 cells were seeded in 6-well plates at 2.5×10^5 cells per well in DMEM media supplemented with 10% FBS and 10 mM glucose, and incubated overnight before treatment with either octanol (vehicle control) or octyl α -KG for 72 h. Cells were lysed in M-PER buffer with protease and phosphatase inhibitors. Lysates were subjected to SDS-PAGE on a 4–12% Bis-Tris gradient gel with MES running buffer and western blotted for LC3 (Novus, NB100-2220). LC3 is the mammalian homologue of worm LGG-1, and conversion of the soluble LC3-I to the lipidated LC3-II is activated in autophagy, for example, upon starvation⁵⁴.

Pharyngeal pumping rates of *C. elegans* treated with 8 mM α -KG. The pharyngeal pumping rates of 20 wild-type N2 worms per condition were assessed. Pharyngeal contractions were recorded for 1 min using a Zeiss M2 BioDiscovery microscope and an attached Sony NDR-XR500V video camera at 12-fold optical zoom. The resulting videos were played back at 0.3× speed using MPlayerX and pharyngeal pumps were counted. Statistical analysis was performed using Microsoft Excel (*t*-test, two-tailed, two-sample unequal variance).

Assay for α -KG levels in *C. elegans*. Synchronized adult worms were collected from plates with vehicle (H_2O) or 8 mM α -KG, washed three times with M9 buffer, and flash frozen. Worms were lysed in M9 using Lysing Matrix C tubes (MP Biomedicals, 6912-100) and the FastPrep-24 (MP Biomedicals) high-speed bench-top homogenizer in the 4 °C room (disrupt worms for 20 s at 6.5 m s^{-1} , rest on ice for 1 min; repeat three times). Lysed animals were centrifuged at 14,000 r.p.m. for 10 min at 4 °C to pellet worm debris, and the supernatant was saved. The protein concentration of the supernatant was determined by the BCA Protein Assay kit (Pierce, 23223); there was no difference in protein level per worm in α -KG-treated and vehicle-treated animals (data not shown). α -KG content was assessed as described previously⁵⁵ with modifications. Worm lysates were incubated at 37 °C in 100 mM KH_2PO_4 (pH 7.2), 10 mM NH_4Cl , 5 mM MgCl_2 and 0.3 mM NADH for 10 min. Glutamate dehydrogenase (Sigma, G2501) was then added to reach a final concentration of 1.83 units ml^{-1} . Under these conditions, glutamate dehydrogenase uses α -KG and NADH to make glutamate. The absorbance decrease was monitored at 340 nm. The intracellular level of α -KG was determined from the absorbance decrease in NADH. The approximate molarity of α -KG present inside the animals was estimated using average protein content (~245 ng per worm, from BCA assay) and volume (~3 nl for adult worms 1.1 mm in length and 60 μm in diameter (<http://www.wormatlas.org/hermaphrodite/introduction/Introframeset.html>)).

For quantitative analysis of α -KG in worms using ultra-high-performance liquid chromatography-electrospray ionization-tandem mass spectrometry (UHPLC-ESI/MS/MS), synchronized day 1 adult worms were placed on vehicle plates with or without bacteria for 24 h, and then collected and lysed in the same manner as described earlier. α -KG analysis by LC/MS/MS was carried out on an Agilent 1290 Infinity UHPLC system and 6460 Triple Quadrupole mass spectrometer (Agilent Technologies) using an electrospray ionization (ESI) source with Agilent Jet Stream technology. Data were acquired with Agilent MassHunter Data Acquisition software version B.06.00, and processed for precursor and product ions selection with MassHunter Qualitative Analysis software version B.06.00 and for calibration and quantification with MassHunter Quantitative Analysis for QQQ software version B.06.00.

For UHPLC, 3 μl calibration standards and samples were injected onto the UHPLC system including a G4220A binary pump with a built-in vacuum degasser and a thermostatted G4226A high performance autosampler. An ACQUITY UPLC BEH Amide analytical column (2.1 × 50 mm, 1.7 μm) and VanGuard BEH Amide Pre-column (2.1 × 5 mm, 1.7 μm) from Waters Corporation were used at the flow rate of 0.6 ml min^{-1} using 50/50/0.04 acetonitrile/water/ammonium hydroxide with 10 mM ammonium acetate as mobile phase A and 95/5/0.04 acetonitrile/water/ammonium hydroxide with 10 mM ammonium acetate as mobile phase B. The column was maintained at room temperature. The following gradient was applied: 0–0.41 min: 100% B isocratic; 0.41–5.30 min: 100–30% B; 5.30–5.35 min: 30–0% B; 5.35–7.35 min: 0% B isocratic; 7.35–7.55 min: 0–100% B; 7.55–9.55 min: 100% B isocratic.

For the MS detection, the ESI mass spectra data were recorded on a negative ionization mode by MRM. MRM transitions of α -KG and its ISTD $^{13}\text{C}_4$ - α -KG (Cambridge Isotope Laboratories) were determined using a 1 min 37% B isocratic UHPLC method through the column at a flow rate of 0.6 ml min^{-1} . The precursor ion of [M-H]⁻ and the product ion of [M-CO₂-H]⁻ were observed to have the highest signal-to-noise ratios. The precursor and product ions are respectively 145.0 and 100.9 for α -KG, and 149.0 and 104.9 for ISTD $^{13}\text{C}_4$ - α -KG. Nitrogen was used as the drying, sheath and collision gas. All the source and analyser parameters were optimized using Agilent MassHunter Source and iFunnel Optimizer and Optimizer software, respectively. The source parameters are as follows: drying gas temperature 120 °C, drying gas flow 13 l min^{-1} , nebulizer pressure 55 psi, sheath gas temperature 400 °C, sheath gas flow 12 l min^{-1} , capillary voltage 2,000 V, and nozzle voltage 0 V. The analyser parameters are as follows: fragmentor voltage 55 V, collision energy 2 V and cell accelerator voltage 1 V. The UHPLC eluants before 1 min and after 5.3 min were diverted to waste.

Membrane-permeable esters of α -KG. Octyl α -KG, a commonly used membrane-permeable ester of α -KG^{55–58}, was used to deliver α -KG across lipid membranes in experiments using cells and mitochondria. Upon hydrolysis by cellular esterases, octyl α -KG yields α -KG and the by-product octanol. We showed that, whereas octanol control has no effect (Extended Data Fig. 2e, f and Extended Data Fig. 6a), α -KG alone can bind and inhibit ATP synthase (Fig. 2a, b and Extended Data Fig. 2a, b; data not shown), decrease ATP and OCR (Fig. 2e, g), induce autophagy (Fig. 4b) and increase *C. elegans* lifespan (Figs 1, 3, Extended Data Figs 1, 5 and Extended Data Table 2). The existence and activity of esterases in our mitochondrial and cell culture experiments have been confirmed using calcein AM (C1430, Molecular Probes), an esterase substrate that fluoresces upon hydrolysis, and also by mass spectrometry (data not shown). The hydrolysis by esterases explains why distinct esters of α -KG, such as 1-octyl α -KG, 5-octyl α -KG, and dimethyl α -KG, have similar effects to α -KG (Extended Data Fig. 2g, h and Extended Data Table 2).

Synthesis of octyl α -KG. Synthesis of 1-octyl α -KG has been previously described⁵⁹. Briefly, 1-octanol (0.95 ml, 6.0 mmol), DMAP (37 mg, 0.3 mmol) and DCC (0.743 g, 3.6 mmol) were added to a solution of 1-cyclobutene-1-carboxylic acid (0.295 g, 3.0 mmol) in dry CH_2Cl_2 (6.0 ml) at 0 °C. After it had been stirred for 1 h, the solution was allowed to warm to room temperature and stirred for another 8 h. The precipitate was filtered and washed with ethyl acetate (3 × 100 ml). The combined organic phases were washed with water and brine, and dried over anhydrous Na_2SO_4 . Flash column chromatography on silica gel eluting with 80/1 hexane/ethyl acetate gave octyl cyclobut-1-enecarboxylate as a clear oil (0.604 g, 96%). To a –78 °C solution of this oil (0.211 g, 1.0 mmol) in CH_2Cl_2 (10 ml) was bubbled O_3/O_2 until the solution turned blue. The residual ozone was discharged by bubbling with O_2 and the reaction was warmed to room temperature and stirred for another 1 h. Dimethyl sulphide (Me_2S , 0.11 ml, 1.5 mmol) was added to the mixture and it was stirred for another 2 h. The CH_2Cl_2 was removed *in vacuo* and the crude product was dissolved in a solution of 2-methyl-2-butene (0.8 ml) in *t*-BuOH (3.0 ml). To this was added dropwise a solution containing sodium chloride (0.147 g, 1.3 mmol) and sodium dihydrogen phosphate monohydrate (0.179 g, 1.3 mmol) in H_2O (1.0 ml). The mixture was stirred at room temperature overnight, and then extracted with ethyl acetate (3 × 50 ml). The combined organic phases were washed with water and brine, and dried over anhydrous Na_2SO_4 . Flash column chromatography on silica gel eluting with 5/1 hexane/ethyl acetate gave octyl α -KG, which became a pale solid when stored in the refrigerator (0.216 g, 84%).

Synthesis of 5-octyl L-glutamate. L-Glutamic acid (0.147 g, 1.0 mmol) and anhydrous sodium sulphate (0.1 g) was dissolved in octanol (2.0 ml), and then tetrafluoroboric acid-dimethyl ether complex (0.17 ml) was added. The suspended mixture was stirred at 21 °C overnight. Anhydrous THF (5 ml) was added to the mixture and it was filtered through a thick pad of activated charcoal. Anhydrous triethylamine (0.4 ml) was added to the clear filtrate to obtain a milky white slurry. Upon trituration with ethyl acetate (10 ml), the monoester monoacid precipitated. The precipitate was collected, washed with additional ethyl acetate (2 × 5 ml), and dried *in vacuo* to give the desired product, 5-octyl L-glutamate (0.249 g, 96%) as a white solid. ¹H NMR (500 MHz, acetic acid-d₄): δ 4.12 (dd, $J = 6.6, 6.6 \text{ Hz}$, 1H), 4.11 (t, $J = 6.8 \text{ Hz}$, 2H), 2.64 (m, 2H), 2.26 (m, 2H), 1.64 (m, 2H), 1.30 (m, 10H), 0.89 (t, $J = 7.0 \text{ Hz}$, 3H). ¹³C NMR (125 MHz, acetic acid-d₄): δ 175.0, 174.3, 66.3, 55.0, 32.7, 30.9, 30.11, 30.08, 29.3, 26.7, 26.3, 23.4, 14.4.

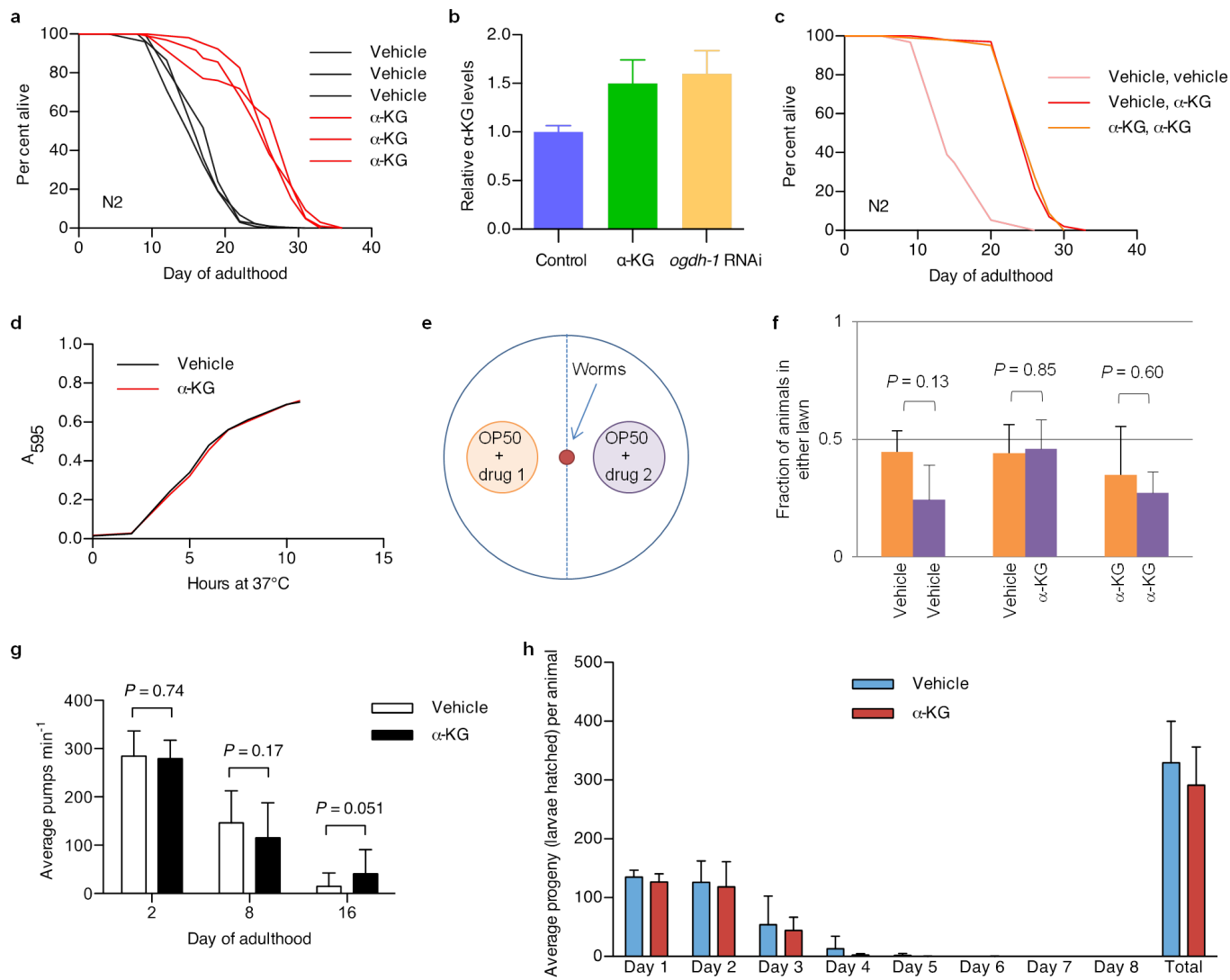
Synthesis of 5-octyl D-glutamate. The synthesis of the opposite enantiomer, that is, 5-octyl D-glutamate, was carried out by the exact same procedure starting with D-glutamic acid. The spectroscopic data was identical to that of the enantiomeric compound.

Synthesis of 5-octyl α -KG. 1-Benzyl 5-octyl 2-oxopentanedioate was obtained as follows. To a solution of 5-octyl L-glutamate (0.249 g) in H_2O (6.0 ml) and acetic acid (2.0 ml) cooled to 0 °C was added slowly a solution of aqueous sodium nitrite (0.207 g, 3.0 mmol in 4 ml H_2O). The reaction mixture was allowed to warm slowly to room temperature and was stirred overnight. The mixture was concentrated.

The resulting residue was dissolved in DMF (10 ml) and NaHCO₃ (0.42 g, 5.0 mmol) and benzyl bromide (0.242 ml, 2.0 mmol) were added to the mixture. The mixture was stirred at 21 °C overnight and then extracted with ethyl acetate (3 × 30 ml). The combined organic phase was washed with water and brine and dried over anhydrous MgSO₄. Flash column chromatography on silica gel eluting with 7/1 hexanes/ethyl acetate gave the mixed diester 1-benzyl 5-octyl (S)-2-hydroxypentanedioate as a colourless oil. To this oil, dissolved in dichloromethane (10.0 ml), were added NaHCO₃ (0.42 g, 5.0 mmol) and Dess–Martin periodinane (0.509 g, 1.2 mmol), and the mixture was stirred at room temperature for 1 h and then extracted with ethyl acetate (3 × 30 ml). The combined organic phase was washed with water and brine and dried over anhydrous MgSO₄. Flash column chromatography on silica gel eluting with 5/1 hexanes/ethyl acetate gave the desired 1-benzyl 5-octyl 2-oxopentanedioate (0.22 g, 66%) as a white solid. ¹H NMR (500 MHz, CDCl₃): δ 7.38 (m, 5H), 5.27 (s, 2H), 4.05 (t, J = 6.5 Hz, 2H), 3.14 (t, J = 6.5 Hz, 2H), 2.64 (t, J = 6.5 Hz, 2H), 1.59 (m, 2H), 1.28 (m, 10H), 0.87 (t, J = 7.0 Hz, 3H). ¹³C NMR (125 MHz, CDCl₃): δ 192.2, 171.9, 160.1, 134.3, 128.7, 128.6, 128.5, 67.9, 65.0, 34.2, 31.7, 29.07, 29.05, 28.4, 27.5, 25.7, 22.5, 14.0.

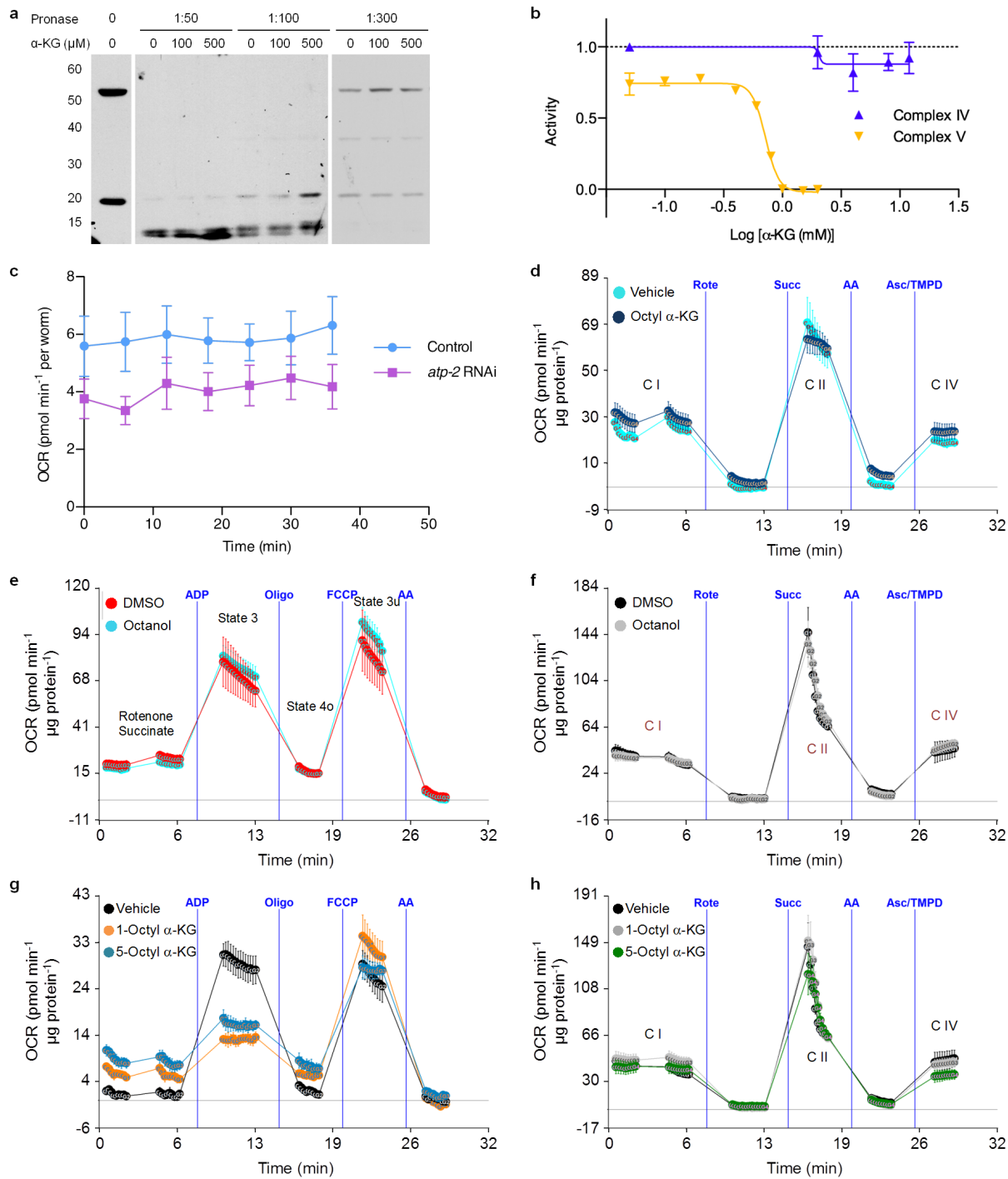
5-Octyl α-KG (5-(octyloxy)-2,5-dioxopentanoic acid) was obtained as follows. To a solution of 1-benzyl 5-octyl 2-oxopentanedioate (0.12 g, 0.344 mmol) in ethyl acetate (15 ml) was added 5% Pd/C (80 mg). Over the mixture was passed a stream of argon and then the argon was replaced with hydrogen gas and the mixture was stirred vigorously for 15 min. The mixture was filtered through a thick pad of Celite to give the desired product 5-octyl α-KG (0.088 g, 99%) as white solid. ¹H NMR (500 MHz, CDCl₃): δ 8.16 (br s, 1H), 4.06 (t, J = 6.5 Hz, 2H), 3.18 (t, J = 6.5 Hz, 2H), 2.69 (t, J = 6.0 Hz, 2H), 1.59 (m, 2H), 1.26 (m, 10H), 0.85 (t, J = 7.0 Hz, 3H). ¹³C NMR (125 MHz, CDCl₃): δ 193.8, 172.7, 160.5, 65.5, 33.0, 31.7, 29.08, 29.06, 28.4, 27.8, 25.8, 22.5, 14.0.

31. Brenner, S. The genetics of *Caenorhabditis elegans*. *Genetics* **77**, 71–94 (1974).
32. Timmons, L. & Fire, A. Specific interference by ingested dsRNA. *Nature* **395**, 854 (1998).
33. Long, X. et al. TOR deficiency in *C. elegans* causes developmental arrest and intestinal atrophy by inhibition of mRNA translation. *Curr. Biol.* **12**, 1448–1461 (2002).
34. Sutphin, G. L. & Kaeberlein, M. Measuring *Caenorhabditis elegans* life span on solid media. *J. Vis. Exp.* **27**, 1152 (2009).
35. Gaudet, J. & Mango, S. E. Regulation of organogenesis by the *Caenorhabditis elegans* FoxA protein PHA-4. *Science* **295**, 821–825 (2002).
36. Abada, E. A. et al. *C. elegans* behavior of preference choice on bacterial food. *Mol. Cells* **28**, 209–213 (2009).
37. Lomenick, B., Jung, G., Wohlschlegel, J. A. & Huang, J. Target identification using drug affinity responsive target stability (DARTS). *Curr. Protoc. Chem. Biol.* **3**, 163–180 (2011).
38. Lomenick, B., Olsen, R. W. & Huang, J. Identification of direct protein targets of small molecules. *ACS Chem. Biol.* **6**, 34–46 (2011).
39. Stubbs, C. J. et al. Application of a proteolysis/mass spectrometry method for investigating the effects of inhibitors on hydroxylase structure. *J. Med. Chem.* **52**, 2799–2805 (2009).
40. Rogers, G. W. et al. High throughput microplate respiratory measurements using minimal quantities of isolated mitochondria. *PLoS ONE* **6**, e21746 (2011).
41. Alberts, B. *Molecular Biology of the Cell* 3rd edn (Garland, 1994).
42. Wu, M. et al. Multiparameter metabolic analysis reveals a close link between attenuated mitochondrial bioenergetic function and enhanced glycolysis dependency in human tumor cells. *Am. J. Physiol. Cell Physiol.* **292**, C125–C136 (2007).
43. Yamamoto, H. et al. NCoR1 is a conserved physiological modulator of muscle mass and oxidative function. *Cell* **147**, 827–839 (2011).
44. Pathare, P. P., Lin, A., Bornfeldt, K. E., Taubert, S. & Van Gilst, M. R. Coordinate regulation of lipid metabolism by novel nuclear receptor partnerships. *PLoS Genet.* **8**, e1002645 (2012).
45. Pullen, N. & Thomas, G. The modular phosphorylation and activation of p70s6k. *FEBS Lett.* **410**, 78–82 (1997).
46. Burnett, P. E., Barrow, R. K., Cohen, N. A., Snyder, S. H. & Sabatini, D. M. RAFT1 phosphorylation of the translational regulators p70 S6 kinase and 4E-BP1. *Proc. Natl. Acad. Sci. USA* **95**, 1432–1437 (1998).
47. Gingras, A. C. et al. Hierarchical phosphorylation of the translation inhibitor 4E-BP1. *Genes Dev.* **15**, 2852–2864 (2001).
48. Sarbassov, D. D., Guertin, D. A., Ali, S. M. & Sabatini, D. M. Phosphorylation and regulation of Akt/PKB by the rictor-mTOR complex. *Science* **307**, 1098–1101 (2005).
49. Kim, J., Kundu, M., Viollet, B. & Guan, K. L. AMPK and mTOR regulate autophagy through direct phosphorylation of Ulk1. *Nature Cell Biol.* **13**, 132–141 (2011).
50. Kang, C., You, Y. J. & Avery, L. Dual roles of autophagy in the survival of *Caenorhabditis elegans* during starvation. *Genes Dev.* **21**, 2161–2171 (2007).
51. Hansen, M. et al. A role for autophagy in the extension of lifespan by dietary restriction in *C. elegans*. *PLoS Genet.* **4**, e24 (2008).
52. Alberti, A., Michelet, X., Djeddi, A. & Legouis, R. The autophagosomal protein LGG-2 acts synergistically with LGG-1 in dauer formation and longevity in *C. elegans*. *Autophagy* **6**, 622–633 (2010).
53. Schneider, C. A., Rasband, W. S. & Eliceiri, K. W. NIH Image to ImageJ: 25 years of image analysis. *Nature Methods* **9**, 671–675 (2012).
54. Kabeya, Y. et al. LC3, a mammalian homologue of yeast Apg8p, is localized in autophagosome membranes after processing. *EMBO J.* **19**, 5720–5728 (2000).
55. Mackenzie, E. D. et al. Cell-permeating α-ketoglutarate derivatives alleviate pseudohypoxia in succinate dehydrogenase-deficient cells. *Mol. Cell. Biol.* **27**, 3282–3289 (2007).
56. Zhao, S. et al. Glioma-derived mutations in IDH1 dominantly inhibit IDH1 catalytic activity and induce HIF-1α. *Science* **324**, 261–265 (2009).
57. Xu, W. et al. Oncometabolite 2-hydroxyglutarate is a competitive inhibitor of α-ketoglutarate-dependent dioxygenases. *Cancer Cell* **19**, 17–30 (2011).
58. Jin, G. et al. Disruption of wild-type IDH1 suppresses D-2-hydroxyglutarate production in IDH1-mutated gliomas. *Cancer Res.* **73**, 496–501 (2013).
59. Jung, M. E. & Deng, G. Synthesis of the 1-monooester of 2-ketoalkanedioic acids, for example, octyl α-ketoglutarate. *J. Org. Chem.* **77**, 11002–11005 (2012).



Extended Data Figure 1 | Supplementation with α-KG extends *C. elegans* adult lifespan but does not change the growth rate of bacteria, or food intake, pharyngeal pumping rate or brood size of the worms. **a**, Robust lifespan extension in adult *C. elegans* by α-KG. 8 mM α-KG increased the mean lifespan of N2 by an average of 47.3% in three independent experiments ($P < 0.0001$ for every experiment, by log-rank test). Experiment 1, mean lifespan (days of adulthood) with vehicle treatment (m_{veh}) = 18.9 ($n = 87$ animals tested), $m_{\alpha\text{-KG}} = 25.8$ ($n = 96$); experiment 2, $m_{\text{veh}} = 17.5$ ($n = 119$), $m_{\alpha\text{-KG}} = 25.4$ ($n = 97$); experiment 3, $m_{\text{veh}} = 16.3$ ($n = 100$), $m_{\alpha\text{-KG}} = 26.1$ ($n = 104$). **b**, Worms supplemented with 8 mM α-KG and worms with RNAi knockdown of α-KGDH (encoded by *ogdh-1*) have increased α-KG levels. Young adult worms were placed on treatment plates seeded with control HT115 *E. coli* or HT115-expressing *ogdh-1* dsRNA, and α-KG content was assayed after 24 h (see Methods). **c**, α-KG treatment beginning at the egg stage and that beginning in adulthood produced identical lifespan increases. Light red, treatment with vehicle control throughout larval and adult stages ($m = 15.6$, $n = 95$); dark red, treatment with vehicle during larval stages and with 8 mM α-KG at adulthood ($m = 26.3$, $n = 102$), $P < 0.0001$ (log-rank test); orange, treatment with 8 mM α-KG throughout larval and adult stages ($m = 26.3$, $n = 102$), $P < 0.0001$ (log-rank test). **d**, α-KG does not alter the

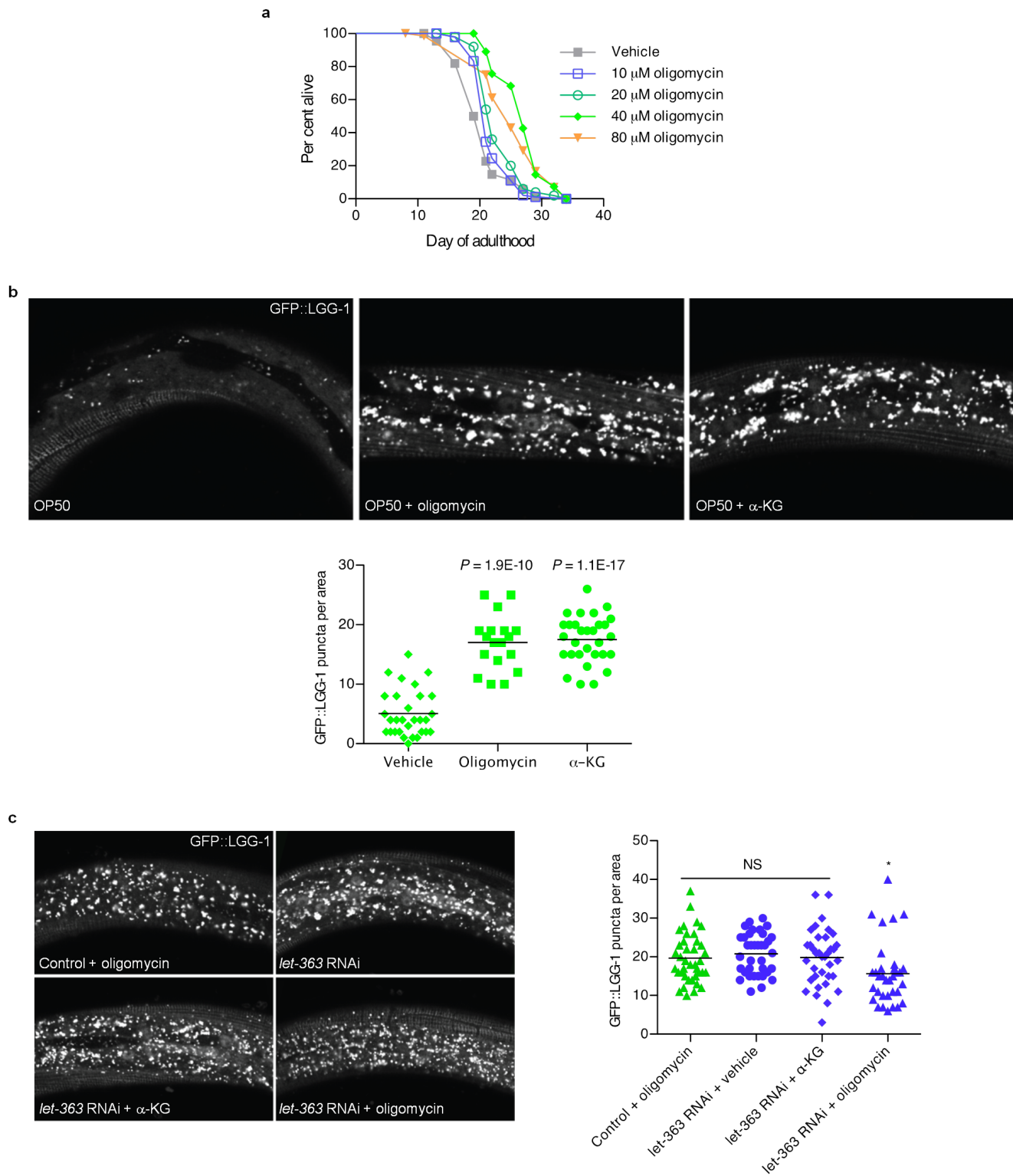
growth rate of the OP50 *E. coli*, which is the standard laboratory food source for nematodes. α-KG (8 mM) or vehicle (H_2O) was added to standard LB media and the pH was adjusted to 6.6 by the addition of NaOH. Bacterial cells from the same overnight OP50 culture were added to the LB \pm α-KG mixture at a 1:40 dilution, and then placed in the 37 °C incubator shaker at 300 r.p.m. The absorbance at 595 nm was read at 1 h time intervals to generate the growth curve. **e**, Schematic representation of food preference assay. **f**, N2 worms show no preference between OP50 *E. coli* treated with vehicle or α-KG ($P = 0.85$, by *t*-test, two-tailed, two-sample unequal variance), nor preference between identically treated OP50 *E. coli*. **g**, Pharyngeal pumping rate of *C. elegans* on 8 mM α-KG is not significantly altered (by *t*-test, two-tailed, two-sample unequal variance). **h**, Brood size of *C. elegans* treated with 8 mM α-KG. Brood size analysis was conducted at 20 °C. Ten L4 wild-type worms were each singly placed onto an NGM plate containing vehicle or 8 mM α-KG. Worms were transferred one per plate onto a new plate every day, and the eggs laid were allowed to hatch and develop on the previous plate. Hatchlings were counted as a vacuum was used to remove them from the plate. Animals on 8 mM α-KG showed no significant difference in brood size compared with animals on vehicle plates ($P = 0.223$, by *t*-test, two-tailed, two-sample unequal variance). Mean \pm s.d. is plotted in all cases.



Extended Data Figure 2 | α -KG binds to the β subunit of ATP synthase and inhibits the activity of complex V but not the other ETC complexes.

a, Western blot showing protection of the ATP-2 protein from Pronase digestion upon α -KG binding in the DARTS assay. The antibody for human ATP5B (Sigma, AV48185) recognizes the epitope 144 IMNVIGEPIDERGPIKT KQFAPIGHAEAPEFMEMSVQEILVTGKVV DLL $_{193}$ that has 90% identity to the *C. elegans* ATP-2. The lower molecular weight band near 20 kDa is a proteolytic fragment of the full-length protein corresponding to the domain directly bound by α -KG. **b**, α -KG does not affect complex IV activity. Complex IV activity was assayed using the MitoTox OXPHOS Complex IV Activity Kit (Abcam, ab109906). Relative complex IV activity was compared to vehicle (H_2O) controls. Potassium cyanide (Sigma, 60178) was used as a positive control for the assay. Complex V activity was assayed using the MitoTox Complex V OXPHOS Activity Microplate Assay (Abcam, ab109907). **c**, *atp-2* RNAi worms have lower oxygen consumption compared to control (*gfp* in RNAi vector), $P < 0.0001$ (*t*-test, two-tailed, two-sample unequal variance) for

the entire time series (two independent experiments); similar to α -KG-treated worms shown in Fig. 2g. **d**, α -KG does not affect the electron flow through the ETC. Oxygen consumption rate (OCR) from isolated mouse liver mitochondria at basal (pyruvate and malate as complex I substrate and complex II inhibitor, respectively, in the presence of FCCP) and in response to sequential injection of rotenone (Rote; complex I inhibitor), succinate (Succ; complex II substrate), antimycin A (AA; complex III inhibitor), ascorbate/tetramethylphenylenediamine (Asc/TMPD; cytochrome *c* (complex IV) substrate). No difference in complex I (C I), complex II (C II) or complex IV (C IV) respiration was observed after 30 min treatment with 800 μ M octyl α -KG, whereas complex V was inhibited (see Fig. 2h) by the same treatment (two independent experiments). **e**, **f**, No significant difference in coupling (e) or electron flow (f) was observed with either octanol or DMSO vehicle control. **g**, **h**, Treatment with 1-octyl α -KG or 5-octyl α -KG gave identical results in coupling (g) or electron flow (h) assays. Mean \pm s.d. is plotted in all cases.

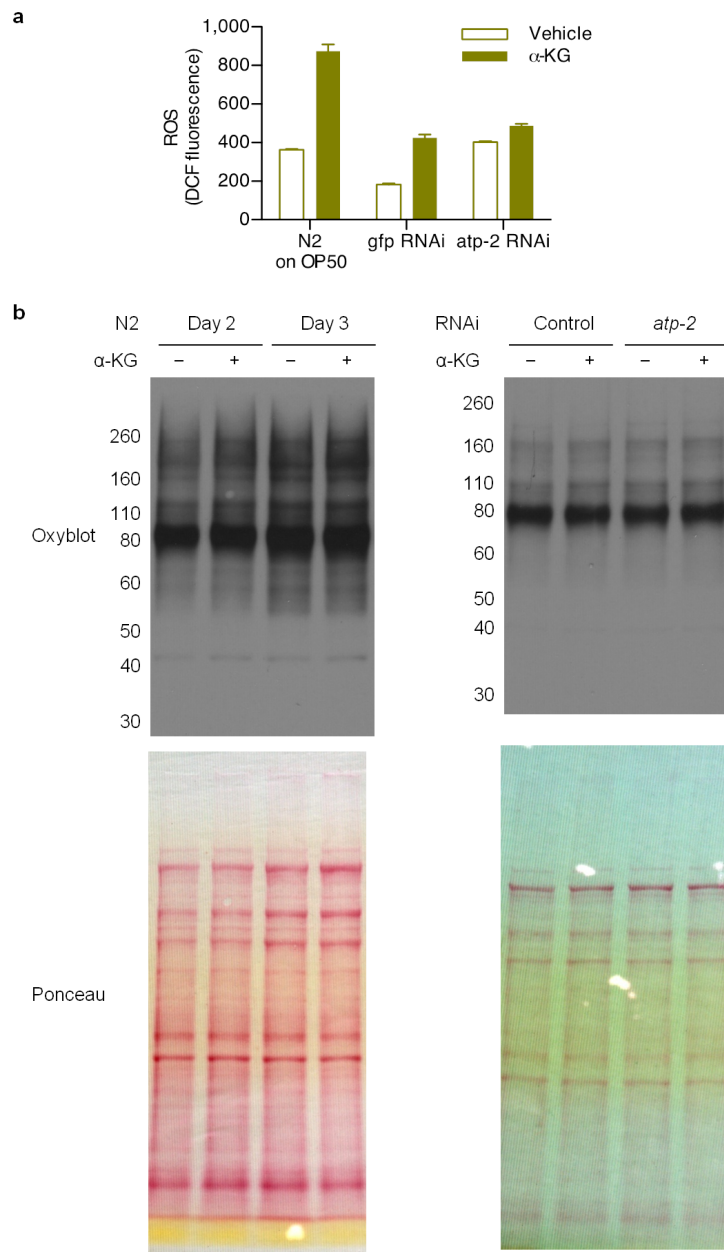


Extended Data Figure 3 | Treatment with oligomycin extends *C. elegans* lifespan and enhances autophagy in a manner dependent on *let-363*.

a. Oligomycin extends the lifespan of adult *C. elegans* in a concentration-dependent manner. Treatment with oligomycin began at the young adult stage. 40 μ M oligomycin increased the mean lifespan of N2 worms by 32.3% ($P < 0.0001$, by log-rank test); see Extended Data Table 2 for details.

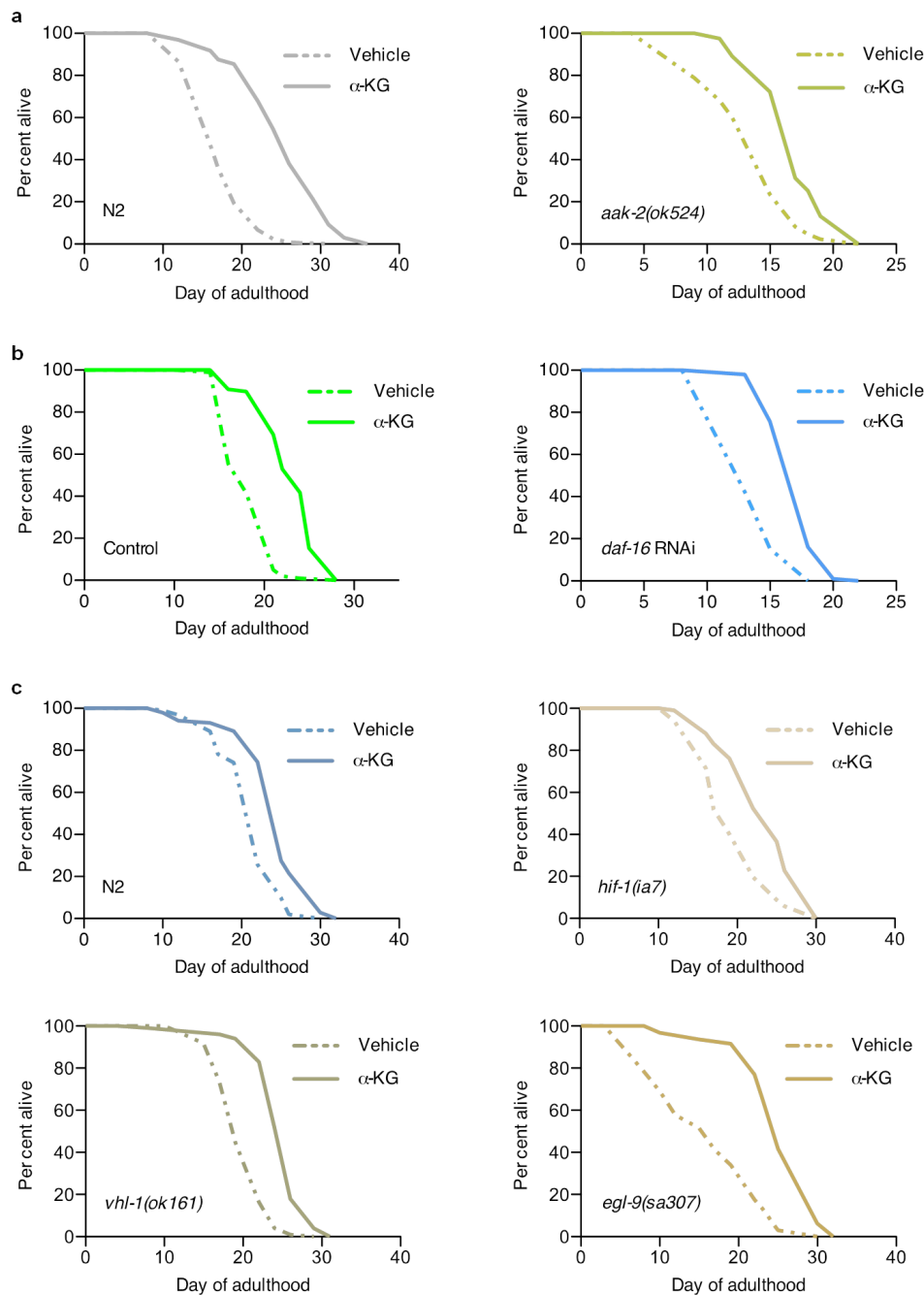
b. Confocal images of GFP::LGG-1 puncta in L3 epidermis of *C. elegans* with vehicle, oligomycin (40 μ M) or α -KG (8 mM), and number of GFP::LGG-1-containing puncta quantified using ImageJ. Bars indicate the mean.

Autophagy in *C. elegans* treated with oligomycin or α -KG is significantly higher than in vehicle-treated control animals (*t*-test, two-tailed, two-sample unequal variance). **c.** There is no significant difference (NS) between control worms treated with oligomycin and *let-363* RNAi worms treated with vehicle, nor between vehicle- and α -KG-treated *let-363* RNAi worms, consistent with independent experiments in Fig. 4b, c; also, oligomycin does not augment autophagy in *let-363* RNAi worms (if anything, there may be a small decrease, as indicated by an asterisk); by *t*-test, two-tailed, two-sample unequal variance. Bars indicate the mean. Photographs were taken at $\times 100$ magnification.



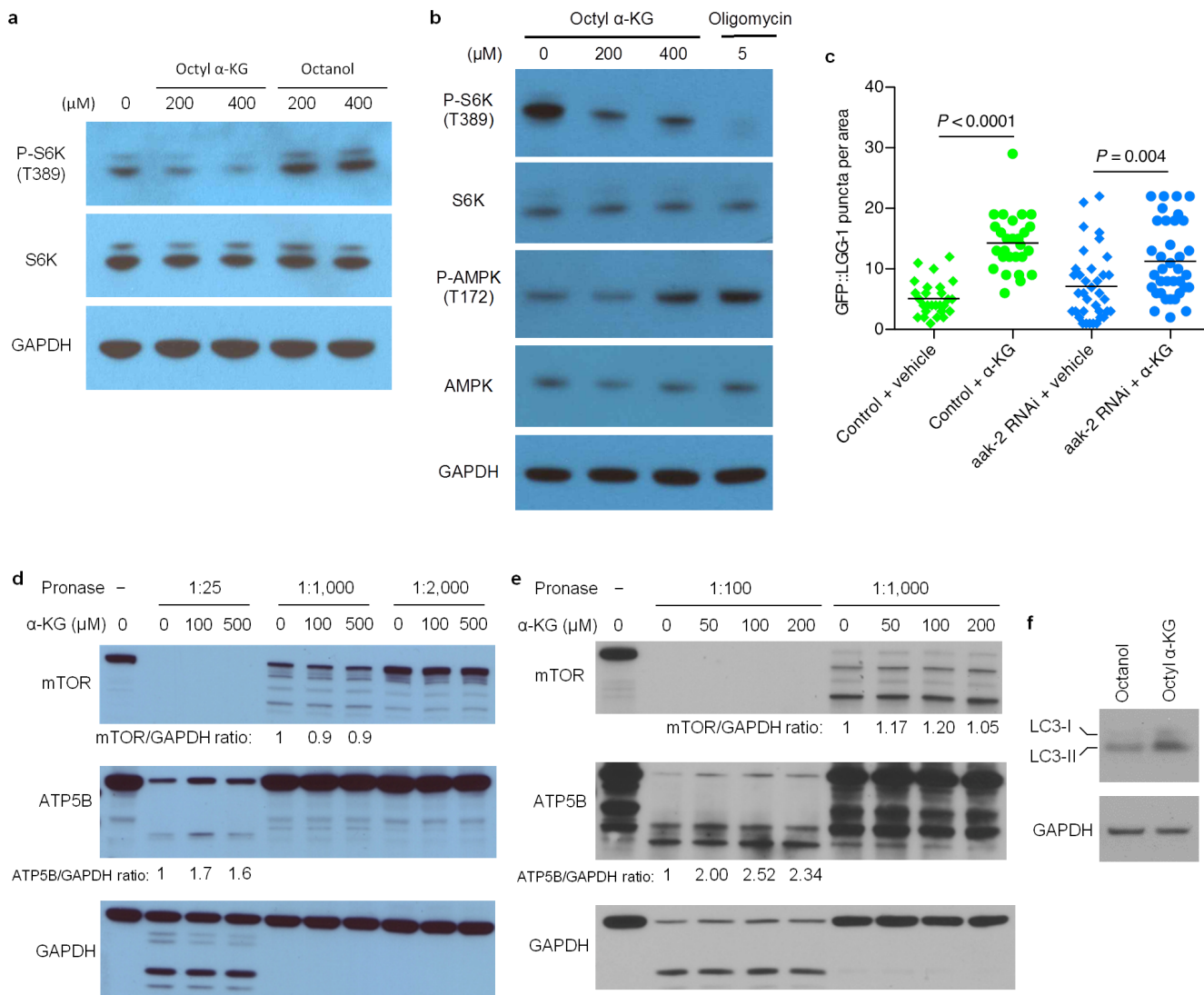
Extended Data Figure 4 | Analyses of oxidative stress in worms treated with α -KG or *atp-2* RNAi. **a**, The *atp-2* RNAi worms have higher levels of 2',7'-dichlorofluorescein (DCF) fluorescence than *gfp* control worms ($P < 0.0001$, by *t*-test, two-tailed, two-sample unequal variance). Supplementation with α -KG also leads to higher DCF fluorescence, in both HT115- (for RNAi) and OP50-fed worms ($P = 0.0007$ and $P = 0.0012$, respectively). Reactive oxygen species (ROS) levels were measured using 2',7'-dichlorodihydrofluorescein diacetate (H₂DCF-DA). As whole worm lysates were used, total cellular oxidative stress was measured here. H₂DCF-DA (Molecular Probes, D399) was dissolved in ethanol to a stock concentration of 1.5 mg ml⁻¹. Fresh stock was prepared every time before use. For measuring ROS in worm lysates, a working concentration of H₂DCF-DA at 30 ng ml⁻¹ was hydrolysed by 0.1 M NaOH at room temperature for 30 min to generate 2',7'-dichlorodihydrofluorescein (DCFH) before mixing with whole worm lysates in a black 96-well plate (Greiner Bio-One). Oxidation of DCFH by ROS yields the highly fluorescent DCF. DCF fluorescence was read at excitation/emission of 485/530 nm using SpectraMax MS (Molecular Devices). H₂O₂ was

used as positive control (data not shown). To prepare the worm lysates, synchronized young adult animals were cultivated on plates containing vehicle or 8 mM α -KG and OP50 or HT115 *E. coli* for 1 day, and then collected and lysed as described in Methods. Mean \pm s.d. is plotted. **b**, There was no significant change in protein oxidation upon α -KG treatment or *atp-2* RNAi. Oxidized protein levels were determined by OxyBlot. Synchronized young adult N2 animals were placed onto plates containing vehicle or 8 mM α -KG, and seeded with OP50 or HT115 bacteria that expressed control or *atp-2* dsRNA. Adult day 2 and day 3 worms were collected and washed four times with M9 buffer, and then stored at -80 °C for at least 24 h. Laemmli buffer (Biorad, 161-0737) was added to every sample and animals were lysed by alternate boil/freeze cycles. Lysed animals were centrifuged at 14,000 r.p.m. for 10 min at 4 °C to pellet worm debris, and supernatant was collected for OxyBlot analysis. Protein concentration of samples was determined by the 660 nm Protein Assay (Thermo Scientific, 1861426) and normalized for all samples. Carbonylation of proteins in each sample was detected using the OxyBlot Protein Oxidation Detection Kit (Millipore, S7150).



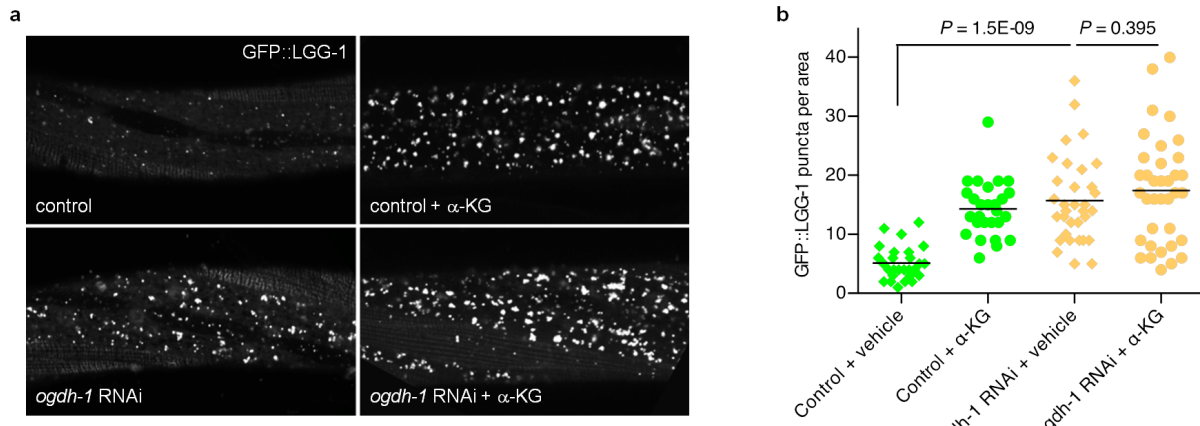
Extended Data Figure 5 | Lifespan extension by α -KG in the absence of *aak-2*, *daf-16*, *hif-1*, *vhl-1* or *egl-9*. **a**, Lifespans of α -KG-supplemented N2 worms, $m_{\text{veh}} = 17.5$ ($n = 119$), $m_{\alpha\text{-KG}} = 25.4$ ($n = 97$), $P < 0.0001$; or *aak-2(ok524)* mutants, $m_{\text{veh}} = 13.7$ ($n = 85$), $m_{\alpha\text{-KG}} = 17.1$ ($n = 83$), $P < 0.0001$. **b**, N2 worms fed *gfp* RNAi control, $m_{\text{veh}} = 18.5$ ($n = 101$), $m_{\alpha\text{-KG}} = 23.1$ ($n = 98$), $P < 0.0001$; or *daf-16* RNAi, $m_{\text{veh}} = 14.3$ ($n = 99$), $m_{\alpha\text{-KG}} = 17.6$ ($n = 99$), $P < 0.0001$. **c**, N2 worms, $m_{\text{veh}} = 21.5$ ($n = 101$), $m_{\alpha\text{-KG}} = 24.6$ ($n = 102$), $P < 0.0001$; *hif-1(ia7)* mutants, $m_{\text{veh}} = 19.6$ ($n = 102$), $m_{\alpha\text{-KG}} = 23.6$ ($n = 101$), $P < 0.0001$; *vhl-1(ok161)* mutants, $m_{\text{veh}} = 20.0$

($n = 98$), $m_{\alpha\text{-KG}} = 24.9$ ($n = 100$), $P < 0.0001$; or *egl-9(sa307)* mutants, $m_{\text{veh}} = 16.2$ ($n = 97$), $m_{\alpha\text{-KG}} = 25.6$ ($n = 96$), $P < 0.0001$. P values were determined by the log-rank test. Number of independent experiments: N2 (8), *hif-1* (5), *vhl-1* (1) and *egl-9* (2); see Extended Data Table 2 for details. Two different *hif-1* mutant alleles²⁷ have been used: *ia4* (shown in Fig. 3g) is a deletion over several introns and exons; *ia7* (shown here) is an early stop codon, causing a truncated protein. Both alleles have the same effect on lifespan²⁷. We tested both alleles for α -KG longevity and obtained the same results.



Extended Data Figure 6 | α -KG decreases TOR pathway activity but does not directly interact with TOR. **a**, Phosphorylation of S6K (T389) was decreased in U87 cells treated with octyl α -KG, but not in cells treated with octanol control. The same results were obtained using HEK-293 and MEF cells. **b**, Phosphorylation of AMPK(T172) is upregulated in WI-38 cells upon complex V inhibition by α -KG, consistent with decreased ATP content in α -KG-treated cells and animals. However, this activation of AMPK appears to require more severe complex V inhibition than the inactivation of mammalian TOR, as either oligomycin or a higher concentration of octyl α -KG was required for increasing phospho (P)-AMPK whereas concentrations of octyl α -KG comparable to those that decreased cellular ATP content (Fig. 2d) or oxygen consumption (Fig. 2f) were also sufficient for decreasing P-S6K. The same results were obtained using U87 cells. Samples were subjected to SDS-PAGE on 4–12% Bis-Tris gradient gel (Invitrogen, NP0322BOX) and western blotted with specific antibodies against P-AMPK T172 (Cell Signaling, 253S) and AMPK (Cell Signaling, 2603S). **c**, α -KG still induces autophagy in *aak-2* RNAi worms; ** $P < 0.01$ (*t*-test, two-tailed, two-sample unequal variance). The number of GFP::LGG-1 containing puncta was quantified using ImageJ. Bars indicate the mean. **d, e**, α -KG does not bind to TOR directly as determined by DARTS. HEK-293 (**d**) or HeLa (**e**) cells were lysed in M-PER buffer (Thermo Scientific, 78501) with the addition of protease inhibitors

(Roche, 11836153001) and phosphatase inhibitors (50 mM NaF, 10 mM β -glycerophosphate, 5 mM sodium pyrophosphate, 2 mM Na₃VO₄). Protein concentration of the lysate was measured by BCA Protein Assay kit (Pierce, 23227). Chilled TNC buffer (50 mM Tris-HCl pH 8.0, 50 mM NaCl, 10 mM CaCl₂) was added to the protein lysate, and the protein lysate was then incubated with vehicle control (DMSO) or varying concentrations of α -KG for 1 h (**d**) or 3 h (**e**) at room temperature. Pronase (Roche, 10165921001) digestions were performed for 20 min at room temperature, and stopped by adding SDS loading buffer and immediately heating at 95 °C for 5 min (**d**) or 70 °C for 10 min (**e**). Samples were subjected to SDS-PAGE on 4–12% Bis-Tris gradient gel (Invitrogen, NP0322BOX) and western blotted with specific antibodies against ATP5B (Santa Cruz, sc58618), mammalian TOR (Cell Signaling, 2972) or GAPDH (Ambion, AM4300). ImageJ was used to quantify the mammalian TOR/GAPDH and ATP5B/GAPDH ratios. Susceptibility of the mammalian TOR protein to Pronase digestion is unchanged in the presence of α -KG, whereas, as expected, Pronase resistance in the presence of α -KG is increased for ATP5B, which we identified as a new binding target of α -KG. **f**, Increased autophagy in HEK-293 cells treated with octyl α -KG was confirmed by western blot analysis of MAP1 LC3 (Novus, NB100-2220), consistent with decreased phosphorylation of the autophagy-initiating kinase ULK1 (Fig. 4a).



Extended Data Figure 7 | Autophagy is enhanced in *C. elegans* treated with *ogdh-1* RNAi. **a**, Confocal images of GFP::LGG-1 puncta in the epidermis of mid-L3 stage, control or *ogdh-1* knockdown *C. elegans* treated with vehicle or α -KG (8 mM). **b**, Number of GFP::LGG-1 puncta quantified using ImageJ.

Bars indicate the mean. *ogdh-1* RNAi worms have significantly higher autophagy levels, and α -KG does not significantly augment autophagy in *ogdh-1* RNAi worms (*t*-test, two-tailed, two-sample unequal variance). Photographs were taken at $\times 100$ magnification.

Extended Data Table 1 | Enriched proteins in the α -KG DARTS sample

Protein Symbol	Protein Name	Score	Control sample		α -KG sample		Enrichment
			Spectra	Peptides	Spectra	Peptides	
ATP5B	ATP synthase subunit beta	4088	23	9	121	15	5.3
HSPD1	60 kDa heat shock protein	2352	31	11	138	29	4.5
PKM2	Pyruvate kinase isozymes M1/M2	2203			56	7	
LCP1	Plastin-2	1865	14	8	76	13	5.4
ATP5A1	ATP synthase subunit alpha	1616	41	9	61	12	1.5
SHMT2	Serine hydroxymethyltransferase	1060	7	5	33	10	4.7
HSP90AA1	Heat shock protein HSP 90-alpha	952	29	8	44	8	1.5
EEF2	Elongation factor 2	943	4	2	37	9	9.3
DDX5	Probable ATP-dependent RNA helicase DDX5	652	7	3	33	10	4.7
HSPA8	Heat shock cognate 71 kDa protein	615	4	2	35	10	8.8

Only showing those proteins with at least 15 spectra in α -KG sample and enriched at least 1.5 fold.

Extended Data Table 2 | Summary of lifespan data

Strain	<i>m</i> (mean lifespan, days)		% difference	<i>P</i> -value	<i>n</i> (number of animals)		
	Vehicle	α -KG			Vehicle	α -KG	
<i>N2</i>	18.9	25.8	36.3	< 0.0001	87	96	
<i>N2</i>	17.5	25.4	45.6	< 0.0001	119	97	
<i>N2</i>	16.3	26.1	60.2	< 0.0001	100	104	
<i>eat-2(ad1116)</i>	22.8	22.9	0.5	0.79	59	40	
<i>daf-16(mu86)</i>	16.3	18.8	15.1	< 0.0001	106	105	
<i>eat-2(ad1116)</i>	21.1	24.0	13.4	0.23	39	59	
<i>daf-2(e1370)</i>	38.0	47.6	25.1	< 0.0001	72	69	
<i>N2</i>	13.2	22.3	69.8	< 0.0001	100	104	
<i>daf-16(mu86)</i>	13.4	17.4	29.5	< 0.0001	71	72	
<i>daf-16 RNAi</i>	14.3	17.6	22.9	< 0.0001	99	99	
<i>N2</i>	16.1	19.1	19.3	0.0003	97	96	
<i>daf-2(e1370)</i>	38.3	43.9	14.6	< 0.0001	109	101	
<i>aak-2(ok524)</i>	13.7	17.1	24.3	< 0.0001	85	83	
<i>aak-2(ok524)</i>	16.4	17.5	6.7	< 0.0001	97	97	
<i>aak-2 RNAi</i>	16.2	19.9	23.3	< 0.0001	93	92	
<i>N2</i>	15.6	26.3	68.8	< 0.0001	95	102	
<i>N2</i>	15.6	26.3	68.5	< 0.0001	95	102	
<i>egl-9(sa307)</i>	16.2	25.6	58.6	< 0.0001	97	96	
<i>egl-9(sa307)</i>	19.5	27.3	40.3	< 0.0001	95	101	
<i>N2</i>	14.7	21.6	46.9	< 0.0001	100	88	
<i>N2</i>	14.0	20.7	47.9	< 0.0001	112	114	
<i>N2</i>	21.5	24.6	14.6	< 0.0001	101	102	
<i>hif-1(ia4)</i>	20.5	26.0	26.5	< 0.0001	85	71	
<i>hif-1(ia7)</i>	19.6	23.6	20.4	< 0.0001	102	101	
<i>hif-1(ia4)</i>	21.5	24.7	14.7	< 0.0001	88	87	
<i>N2</i>	16.7	23.4	39.7	< 0.0001	104	103	
<i>N2</i>	15.8	22.2	40.5	< 0.0001	104	94	
<i>N2</i>	18.4	24.6	33.4	< 0.0001	99	89	
<i>vhl-1(ok161)</i>	20.0	25.0	24.9	< 0.0001	98	100	
<i>hif-1(ia7)</i>	12.4	17.3	38.9	< 0.0001	97	90	
<i>hif-1(ia7)</i>	17.9	23.7	32.0	< 0.0001	58	55	
<i>N2</i>	16.8	22.4	32.7	< 0.0001	104	101	
<i>N2</i>	15.7	21.6	37.6	< 0.0001	85	99	
<i>smg-1(cc546ts)</i>	18.4	23.8	29.5	< 0.0001	110	87	
<i>smg-1(cc546ts);pha-4(zu225)</i>	14.2	13.5	-4.9	0.5482	94	109	
<i>smg-1(cc546ts);pha-4(zu225)</i>	17.6	15.2	-14.0	0.0877	28	34	
<i>N2</i>	13.6	20.7	51.8	< 0.0001	103	104	
<i>smg-1(cc546ts)</i>	16.2	23.0	42.2	< 0.0001	114	121	
<i>smg-1(cc546ts);pha-4(zu225)</i>	13.8	15.2	10.2	0.254	45	45	
EV RNAi control	18.6	23.4	26.1	< 0.0001	94	91	
<i>atp-2</i> RNAi	22.8	22.5	-1.3	0.3471	97	94	
EV RNAi control	18.8	22.7	20.6	< 0.0001	97	94	
gfp RNAi control	18.5	23.1	25.3	< 0.0001	101	98	
<i>ogdh-1</i> RNAi	21.2	21.1	-0.7	0.65	98	100	
<i>let-363</i> RNAi	22.1	23.6	6.8	0.02	94	95	
gfp RNAi control	20.2	27.7	37.4	< 0.0001	99	81	
<i>let-363</i> RNAi	25.1	25.7	2.1	0.9511	96	74	
EV RNAi control	22.8	27.2	21.6	< 0.0001	70	72	
<i>let-363</i> RNAi	27.4	27.2	-0.8	0.7239	64	80	
EV RNAi control	19.7	24.3	23.8	< 0.0001	93	84	
<i>atp-2</i> RNAi	25.3	23.4	-7.4	< 0.0001	87	63	
Strain	<i>m</i>		% difference	<i>P</i> -value	<i>n</i>		[Oligomycin]
	Vehicle	Oligomycin			Vehicle	Oligomycin	
<i>N2</i>		25.5	25.2	< 0.0001	72	80 μ M	
<i>N2</i>	20.4	27.0	32.3	< 0.0001	88	40 μ M	
<i>N2</i>		23.1	13.2	0.0005	50	20 μ M	
<i>N2</i>		22.0	7.9	0.0106	90	10 μ M	
Strain	<i>m</i>		% difference	<i>P</i> -value	<i>n</i>		Treatment
	Vehicle	Treatment			Vehicle	Treatment	
<i>N2</i>	14.5	16.9	16.8	0.0005	73	71 Octyl α -KG (500 μ M)	
<i>N2</i>	14.5	17.0	16.8	< 0.0001	73	60 α -KG	
<i>N2</i>	14.0	18.8	33.9	< 0.0001	112	114 Dimethyl α -KG	
<i>N2</i>	14.0	20.7	47.8	< 0.0001	112	114 α -KG	
<i>N2</i>	15.7	21.6	37.6	< 0.0001	85	99 Disodium α -KG	
Strain	<i>m</i>		% difference	<i>P</i> -value	<i>n</i>		Food source
	Vehicle	α -KG			Vehicle	α -KG	
<i>N2</i>	17.4	21.2	21.6	0.0001	108	55 Live OP50	
<i>N2</i>	19.0	23.0	21.0	0.0003	88	46 Dead OP50 (γ -irradiated)	